



NAVAL POSTGRADUATE SCHOOL

MONTEREY, CALIFORNIA

THESIS

HIGH LATITUDE COUPLED SEA-ICE-AIR THERMODYNAMICS

by

William A. Swick

September 2004

Thesis Advisor:

Roland W. Garwood

Second Reader:

Arlene Guest

Approved for public release; distribution is unlimited

THIS PAGE INTENTIONALLY LEFT BLANK

REPORT DOCUMENTATION PAGE			<i>Form Approved OMB No. 0704-0188</i>	
Public reporting burden for this collection of information is estimated to average 1 hour per response, including the time for reviewing instruction, searching existing data sources, gathering and maintaining the data needed, and completing and reviewing the collection of information. Send comments regarding this burden estimate or any other aspect of this collection of information, including suggestions for reducing this burden, to Washington headquarters Services, Directorate for Information Operations and Reports, 1215 Jefferson Davis Highway, Suite 1204, Arlington, VA 22202-4302, and to the Office of Management and Budget, Paperwork Reduction Project (0704-0188) Washington DC 20503.				
1. AGENCY USE ONLY (Leave blank)		2. REPORT DATE September 2004	3. REPORT TYPE AND DATES COVERED Master's Thesis	
4. TITLE AND SUBTITLE: High latitude coupled sea-ice-air thermodynamics			5. FUNDING NUMBERS	
6. AUTHOR(S) William A. Swick				
7. PERFORMING ORGANIZATION NAME(S) AND ADDRESS(ES) Naval Postgraduate School Monterey, CA 93943-5000			8. PERFORMING ORGANIZATION REPORT NUMBER	
9. SPONSORING /MONITORING AGENCY NAME(S) AND ADDRESS(ES) N/A			10. SPONSORING/MONITORING AGENCY REPORT NUMBER	
11. SUPPLEMENTARY NOTES The views expressed in this thesis are those of the author and do not reflect the official policy or position of the Department of Defense or the U.S. Government.				
12a. DISTRIBUTION / AVAILABILITY STATEMENT Approved for public release; distribution is unlimited			12b. DISTRIBUTION CODE	
13. ABSTRACT (maximum 200 words) Presently ice extent forecast models such as the U.S. Navy Polar Ice Prediction System (PIPS) neglect or treat small-scale thermodynamic processes and entrainment unrealistically. Incorporating better algorithms that include more complete physics of the mixed layer dynamics will allow for improved prediction of ice thickness and distribution, open water boundaries, polynyas, and deep-water formation in the polar seas. A one-dimensional mixed layer turbulent kinetic energy (TKE) budget model based on Garwood's NPS mixed layer model for deep convection (Garwood, 1991) was written in MATLAB®. The model consisted of a system of ten equations derived by vertically integrating the budgets for heat, momentum, salinity, and turbulent kinetic energy between the sea-ice-air interface and the base of the turbulent mixed layer. The NPS mixed layer model was tested using atmospheric forcing and ocean profiles collected at the Surface Heat Budget of the Arctic Ocean Experiment (SHEBA) site. Sensitivity studies using ocean profiles of the Greenland Sea were also conducted to address thermodynamics and ocean profiles that enhance thermohaline circulation. Findings and results as well as recommendations for further study are addressed to extend the relationships determined from small 1-D scales to the larger 3-D scales suitable for improvements to current ice models.				
14. SUBJECT TERMS Mixed Layer, SHEBA, Greenland Sea, Thermobaricity, Entrainment, Air, Sea, Ice, Interaction, Modeling, Arctic Ocean			15. NUMBER OF PAGES 91	
			16. PRICE CODE	
17. SECURITY CLASSIFICATION OF REPORT Unclassified	18. SECURITY CLASSIFICATION OF THIS PAGE Unclassified	19. SECURITY CLASSIFICATION OF ABSTRACT Unclassified	20. LIMITATION OF ABSTRACT UL	

THIS PAGE INTENTIONALLY LEFT BLANK

Approved for public release; distribution is unlimited

HIGH LATITUDE COUPLED SEA-ICE-AIR THERMODYNAMICS

William A. Swick
Lieutenant, United States Navy
B.A., Villanova University, 1996

Submitted in partial fulfillment of the
requirements for the degree of

**MASTER OF SCIENCE IN METEOROLOGY AND PHYSICAL
OCEANOGRAPHY**

from the

**NAVAL POSTGRADUATE SCHOOL
September 2004**

Author: William A. Swick

Approved by: Roland W. Garwood
Thesis Advisor

Arlene Guest
Second Reader

Mary Batteen
Chairman, Department of Oceanography

THIS PAGE INTENTIONALLY LEFT BLANK

ABSTRACT

Presently ice extent forecast models such as the U.S. Navy Polar Ice Prediction System (PIPS) neglect or treat small-scale thermodynamic processes and entrainment unrealistically. Incorporating better algorithms that include more complete physics of the mixed layer dynamics will allow for improved prediction of ice thickness and distribution, open water boundaries, polynyas, and deep-water formation in the polar seas.

A one-dimensional mixed layer turbulent kinetic energy (TKE) budget model based on Garwood's NPS mixed layer model for deep convection (Garwood, 1991) was written in MATLAB®. The model consisted of a system of ten equations derived by vertically integrating the budgets for heat, momentum, salinity, and turbulent kinetic energy between the sea-ice-air interface and the base of the turbulent mixed layer.

The NPS mixed layer model was tested using atmospheric forcing and ocean profiles collected at the Surface Heat Budget of the Arctic Ocean Experiment (SHEBA) site, where wind stress and forced convection predominates. Sensitivity studies using ocean profiles of the Greenland Sea were also conducted to address thermodynamics and ocean profiles, where surface cooling and free convection predominates.

Specific findings and results include: the role of unsteadiness, the responses of feedback processes depending on the mixed layer structure, and the importance of the temporal resolution of the model forcing on both skill and sensitivity of the output. The role of unsteadiness such as heat storage within the mixed layer has a large impact on ice melting or formation. Feedback between the atmosphere and ice is responsive and depends not only on atmospheric forcing but the underlying ocean structure. Feedback is negative for stable ocean profiles such as the Western Arctic but can become positive, promoting deep convection, given weakly stable ocean profiles like that of the Greenland Sea. The importance of model time step is evaluated by comparing output from time-averaged prescribed surface forcing. The long-term goal of this work, and future studies, is to extend the relationships determined from the small 1-D scales to the larger 3-D scales suitable for improvements to current ice models.

THIS PAGE INTENTIONALLY LEFT BLANK

TABLE OF CONTENTS

I.	INTRODUCTION.....	1
II.	POLAR SEAS	3
A.	ARCTIC OCEAN AND ITS MARGINAL SEAS CIRCULATION.....	4
1.	Physiography	4
2.	Circulation	8
B.	MIXED LAYER STRUCTURE	9
1.	Beaufort and Chukchi Seas.....	9
2.	Greenland Sea	11
C.	DEEP CONVECTION	15
1.	Atmospheric Forcing	15
D.	NEAR SURFACE CONDITIONS AND OVERALL ENERGY BUDGET.....	17
1.	SHEBA Atmospheric and Ice Measurement Data.....	18
a.	<i>Winds</i>	21
b.	<i>Total Energy Flux</i>	21
c.	<i>Ice Thickness</i>	25
III.	PROCEDURE	27
A.	MIXED LAYER ICE COUPLE MODEL (MICE)	27
1.	Ocean Mixed Layer Structure	27
2.	Turbulent Kinetic Energy Budget.....	27
a.	<i>Notation</i>	27
b.	<i>Entrainment Hypothesis</i>	28
c.	<i>Integration of TKE</i>	29
3.	1-D Mixed Layer Ice Coupled Model.....	36
IV.	SENSITIVITY STUDIES.....	41
A.	VARYING INITIAL CONDITIONS.....	43
1.	Turbulent Kinetic Energy	43
2.	Mixed Layer Depth, Temperature and Salinity Profile	45
B.	VARYING WIND SPEED WITH THE SAME NET HEAT FLUX	49
C.	VARYING NET HEAT FLUX WITH THE SAME WIND SPEED	53
1.	Simulation for Fifty Days	53
2.	Simulation for One-Hundred and Fifty Days.....	56
D.	ATMOSPHERIC FORCING	60
1.	Retreating Regime	65
V.	CONCLUSIONS	69
A.	SUMMARY	69
B.	RECOMMENDATIONS FOR FURTHER STUDY	70
	LIST OF REFERENCES.....	71
	INITIAL DISTRIBUTION LIST	75

THIS PAGE INTENTIONALLY LEFT BLANK

LIST OF FIGURES

Figure 1.	Polar seas unique temperature and salinity structure.....	3
Figure 2.	Topography and bathymetry of the Arctic (ETOPO5 data set, NOAA 1988).	4
Figure 3.	Winter and summer surface water temperatures (C) in the Arctic Ocean and adjacent seas (USSR Ministry of Defense 1980).....	6
Figure 4.	Winter and summer surface water salinity in the Arctic Ocean and adjacent seas (USSR Ministry of Defense 1980).....	7
Figure 5.	Surface ocean currents in the Arctic.	8
Figure 6.	A schematic of the circulation over the Chukchi Sea and Beaufort/Chukchi slope (Weingartner, 2004)	10
Figure 7.	Beaufort and Chukchi Sea variable T/S profiles over the SHEBA study.....	11
Figure 8.	Representative Greenland Sea T-S profiles, from observations by Quadfasel and Ungewiß (1988).....	12
Figure 9.	Western Arctic T/S profile comparison, from SHEBA (1997).....	13
Figure 10.	When ice is present all entrained heat is fluxed into the ice (Garwood, 2004).	14
Figure 11.	Mean sea-level pressure for January in the Arctic (AMAP Assessment Report, 1998)	16
Figure 12.	Mean sea-level pressure for July in the Arctic (AMAP Assessment Report, 1998).	17
Figure 13.	SHEBA ice floe drifted more than 1400 km in the Beaufort and Chukchi Seas (SHEBA Map of Ice Station Drift, 2004).....	18
Figure 14.	SHEBA atmospheric data	19
Figure 15.	SHEBA ocean and ice measurement data.....	20
Figure 16.	SHEBA temperature and salinity profiles of the ocean to 150 m.....	21
Figure 17.	The surface is considered as a slab of snow and ice	22
Figure 18.	Heat Flux Components	24
Figure 19.	Sensible heat flux and latent heat flux warming the surface during the winter and weakly cooling during the summer time.....	25
Figure 20.	Linear variation of the thermal expansion coefficient with temperature, salinity and pressure.....	31
Figure 21.	Dependence of H_α on potential temperature and salinity.....	32
Figure 22.	Sensitivity to varying TKE - Greenland Sea Julian Day 308-318.	44
Figure 23.	TKE Convergence at 0.5 Day- Greenland Sea Julian Day 308-318.....	45
Figure 24.	Representative Ocean Structure for Western Arctic and Greenland Sea.....	46
Figure 25.	Sensitivity to Initial conditions: h, T(z), S(z).	47
Figure 26.	Heat storage for both the Greenland Sea and Western Arctic mixed layer.	48
Figure 27.	Difference of mixed layer temperature from the freezing point is an order of magnitude smaller than the TKE in the system.....	49
Figure 28.	Varying Wind Speed same Net Heat Flux	51
Figure 29.	Total TKE and vertical TKE for vary wind speed.....	52

Figure 30.	Sensitivity of net heat flux out and heat provided to the ice from the ocean...	53
Figure 31.	Three time series of net heat flux forcing during simulation.....	54
Figure 32.	Varying net heat flux for the same wind speed.....	55
Figure 33.	Total TKE and vertical TKE for vary net heat flux.....	56
Figure 34.	Ice melting despite atmospheric cooling.....	57
Figure 35.	Entrainment is damped in response to the negative buoyancy flux in the mixed layer resulting from ice melting.....	58
Figure 36.	Ice transitioning on short time scales between freezing and melting periods in response to the atmosphere forcing and ocean feedback.....	59
Figure 37.	Damping effect on vertical TKE due to the ice melting.....	59
Figure 38.	Moving average applied to wind forcing.....	60
Figure 39.	Moving average applied to net heat flux.....	61
Figure 40.	Western Arctic MICE simulation	62
Figure 41.	Greenland Sea MICE simulation	63
Figure 42.	Western Arctic Total TKE	64
Figure 43.	Greenland Sea Total TKE	65
Figure 44.	Greenland Sea Daily Forcing Total TKE.....	66
Figure 45.	Greenland Sea Daily Forcing MICE Model vs. Model verses Retreating Version.....	67

LIST OF TABLES

Table 1.	Table of Values for Physical Constants.....	42
Table 2.	Table of Surface Boundary and Below-Layer Forcing Conditions	43

THIS PAGE INTENTIONALLY LEFT BLANK

ACKNOWLEDGMENTS

I would like to thank Dr. Garwood for his help and direction throughout this thesis study. Time after time, his easy grasp of physics at its most fundamental level helped me in the struggle for my own understanding. Thanks as well to Ms. Arlene Guest for answering my numerous computer questions, and her guidance throughout my graduate study. Finally, I would like to thank those closest to me, my family, whose presence helped make the completion of my graduate work possible. I especially thank Laura, my wife and best friend for the past 6 years whose support and love has been unwavering, and my daughter Maeve, and son Liam, who are my joy and my happiness.

THIS PAGE INTENTIONALLY LEFT BLANK

I. INTRODUCTION

The scientific objective of this work is to model how the state of the ice cover changes in response to forcing from the atmosphere and the ocean. Presently ice extent forecast models such as the U.S. Navy Polar Ice Prediction System (PIPS) neglect or treat small-scale thermodynamic processes and entrainment unrealistically. Incorporating better algorithms that include more complete physics of the mixed layer dynamics will allow for improved prediction of ice thickness and distribution, open water boundaries, polynyas, and deep-water formation in the polar seas. As a result, the Navy would improve mission planning, effectiveness and efficiency for all operations in the polar regions. Additionally, because the same physical processes that are explored in this work as mechanisms for ice formation and melting also play a significant role in the global climate, the long-term importance of this study goes beyond tactical forecast capabilities and mission effectiveness to include macro-scale circulation and deep-water convection.

The sea-ice-air system in the high latitudes is strongly coupled. Heat and salinity fluxes that determine when, and how much ice will freeze or melt are a result of the sea-ice-air system interaction as a whole; no single factor is most important. Subtle changes in the density structure and circulation of the polar oceans can have significant effects. For that reason differences between the Western Arctic and the Greenland seas will be addressed in order to shed light on thermodynamic properties and structures that enhance thermohaline circulation, thus influencing the vertical mixing of energy, mass and momentum in the polar seas. Model output of both ice thickness and ice extent can be improved by including the atmospheric processes together with the more complete physics of the mixed layer dynamics and the underlying temperature and salinity structure of the ocean.

A one-dimensional mixed layer turbulent kinetic energy (TKE) budget model based on Garwood's NPS mixed layer model for deep convection (Garwood, 1991) was written in MATLAB®. It consisted of a system of ten equations derived by vertically integrating the budgets for heat, momentum, salinity, and turbulent kinetic energy between the sea-ice-air interface and the base of the turbulent mixed layer.

The NPS mixed layer model was tested using atmospheric forcing and ocean profiles collected at the Surface Heat Budget of the Arctic Ocean Experiment (SHEBA) site. Sensitivity studies using ocean profiles of the Greenland Sea from observations by Quadfasel and Ungewiß (1988) will shed light on the subtle thermodynamics and ocean profiles that enhance thermohaline circulation. Findings and results as well as recommendations for further study will be addressed to achieved the ultimate goal, to extend the relationships determined in this work from small 1-D scales to the larger 3-D scales suitable for climate models.

II. POLAR SEAS

This section examines the physical oceanography of the polar seas. The focus will be on the unique temperature and salinity structure (Figure 1) and physical processes that influence the formation and melting of sea ice. The sea ice cover is unique to the polar oceans and affects the physiography in a number of ways: The temperature of the surface water remains near the freezing point as a function of its salinity. The brine rejection due to ice freezing increases the density of the surface waters and enhances thermohaline circulation. Atmospheric winds transfer momentum to the mixed layer through the sea ice cover. The drag coefficient, and thereby the momentum transfer, can vary greatly depending on the character of the ice, e.g. smooth, rough. Lastly, the ice albedo is seasonally variable. This affects the exchange of solar heating at the surface and the energy available to melt the ice cover.

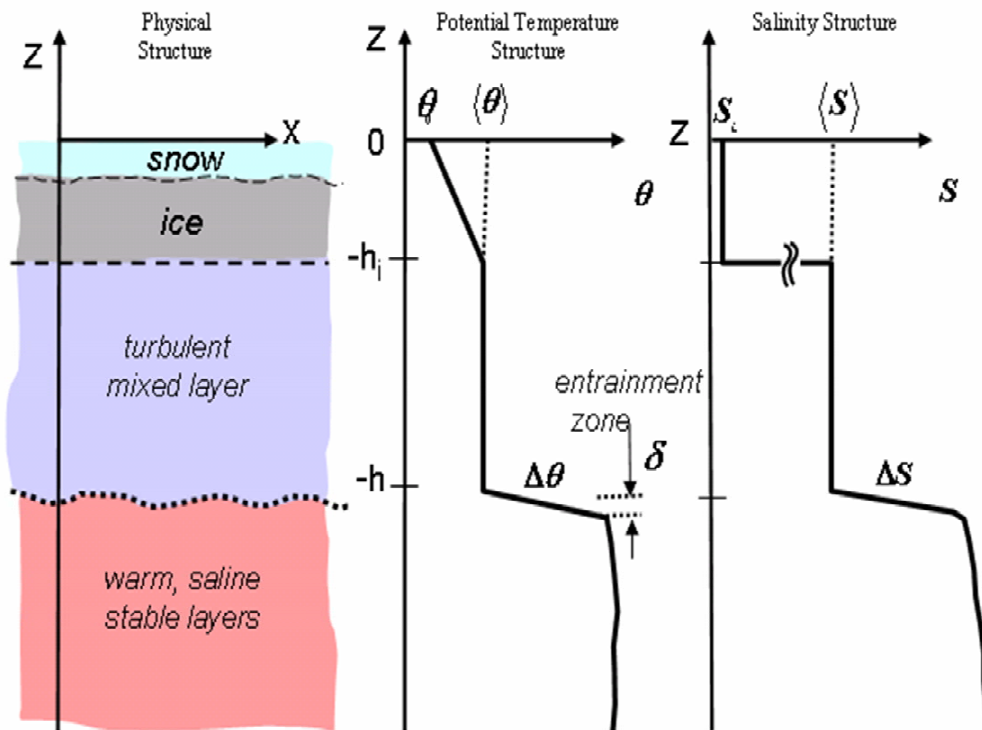


Figure 1. Polar seas unique temperature and salinity structure.

A. ARCTIC OCEAN AND ITS MARGINAL SEAS CIRCULATION

1. Physiography

Connected primarily to the Atlantic Ocean, a lesser-input circulation is from the Bering Strait, which provides a shallow (less than 45m) connection to the Pacific Ocean; the Arctic Ocean is an ocean basin that occupies an area of approximately 12 million square kilometers. An important feature of this ocean basin is the presence of sea ice. Sea ice covers less than 10% of the world's oceans, and 40% of this sea ice occurs within the Arctic Ocean basin. The presence of sea ice and the annual cycle of melting and freezing have a significant effect on the exchanges of mass, momentum and energy of the Arctic Ocean and its marginal seas (Figure 2).

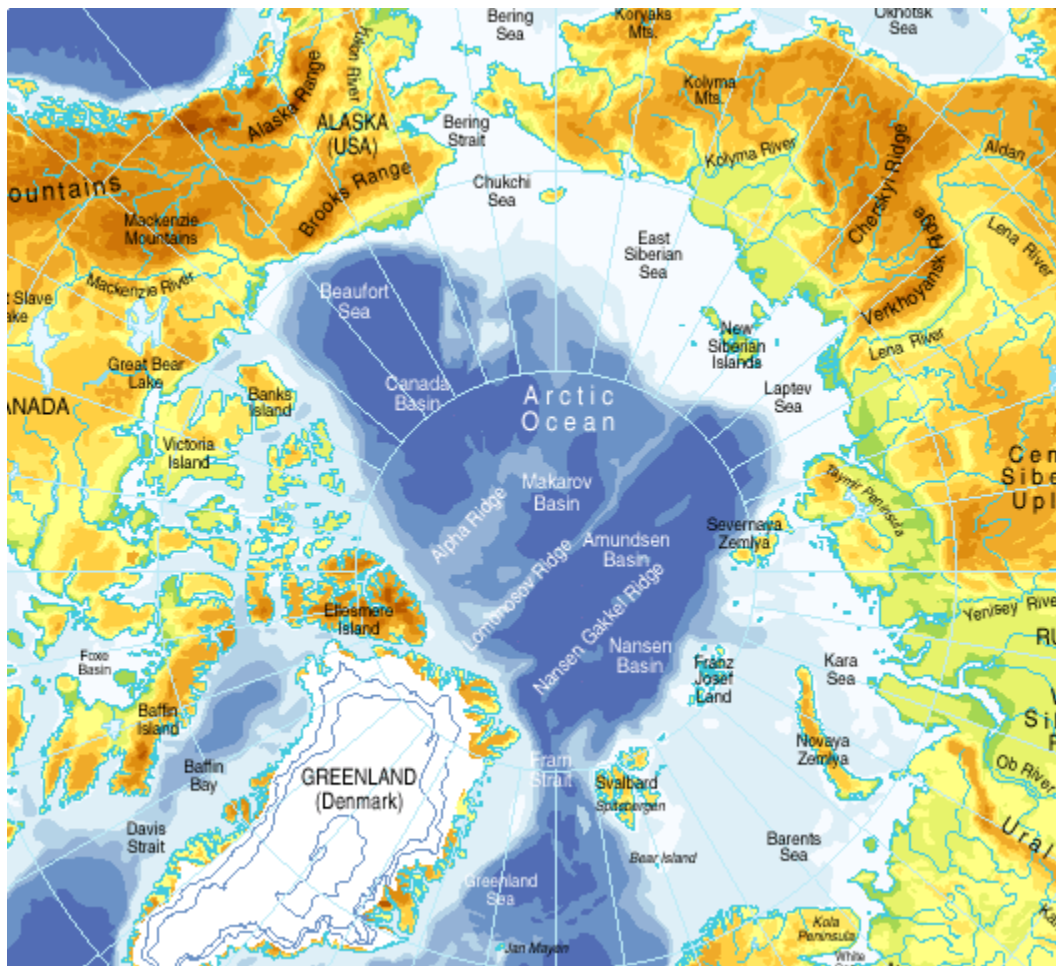


Figure 2. Topography and bathymetry of the Arctic (ETOPO5 data set, NOAA 1988).

The temperature of surface waters in the Arctic Ocean basin varies from -1.5 to -1.9 C (i.e., the freezing point of sea water dependent on the surface salinity). As these surface waters move through the Canadian Arctic Archipelago and Fram Strait, the temperature increases gradually. Here the polar surface waters exhibit temperatures ranging from 3 to -1.9 C (Figure 3).

Surface water salinity in the Arctic Ocean and the marginal seas is relatively low compared to other oceans (Figure 4). In the Arctic Ocean itself, surface salinity varies between 30 and 33, and decreases in the area of the shelf seas in the Western Arctic to below 30. Generally, the salinity is lower during summer than winter due to input of freshwater from river discharge and ice melt. During the winter, the combination of sensible cooling and brine rejection from the ice increases the salinity of the surface water inducing thermohaline circulation (AMAP Assessment Report, 1998).

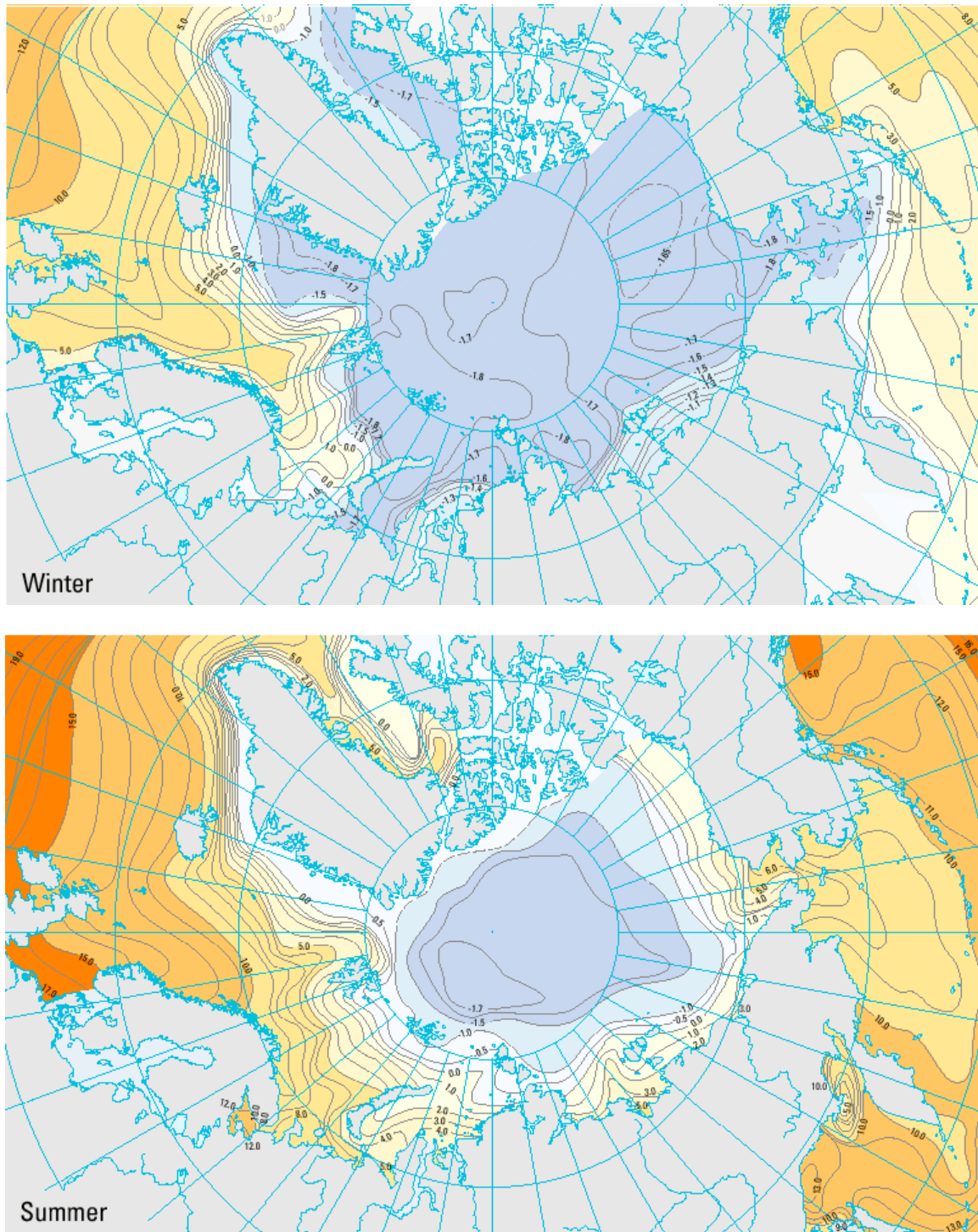


Figure 3. Winter and summer surface water temperatures (C) in the Arctic Ocean and adjacent seas (USSR Ministry of Defense 1980).

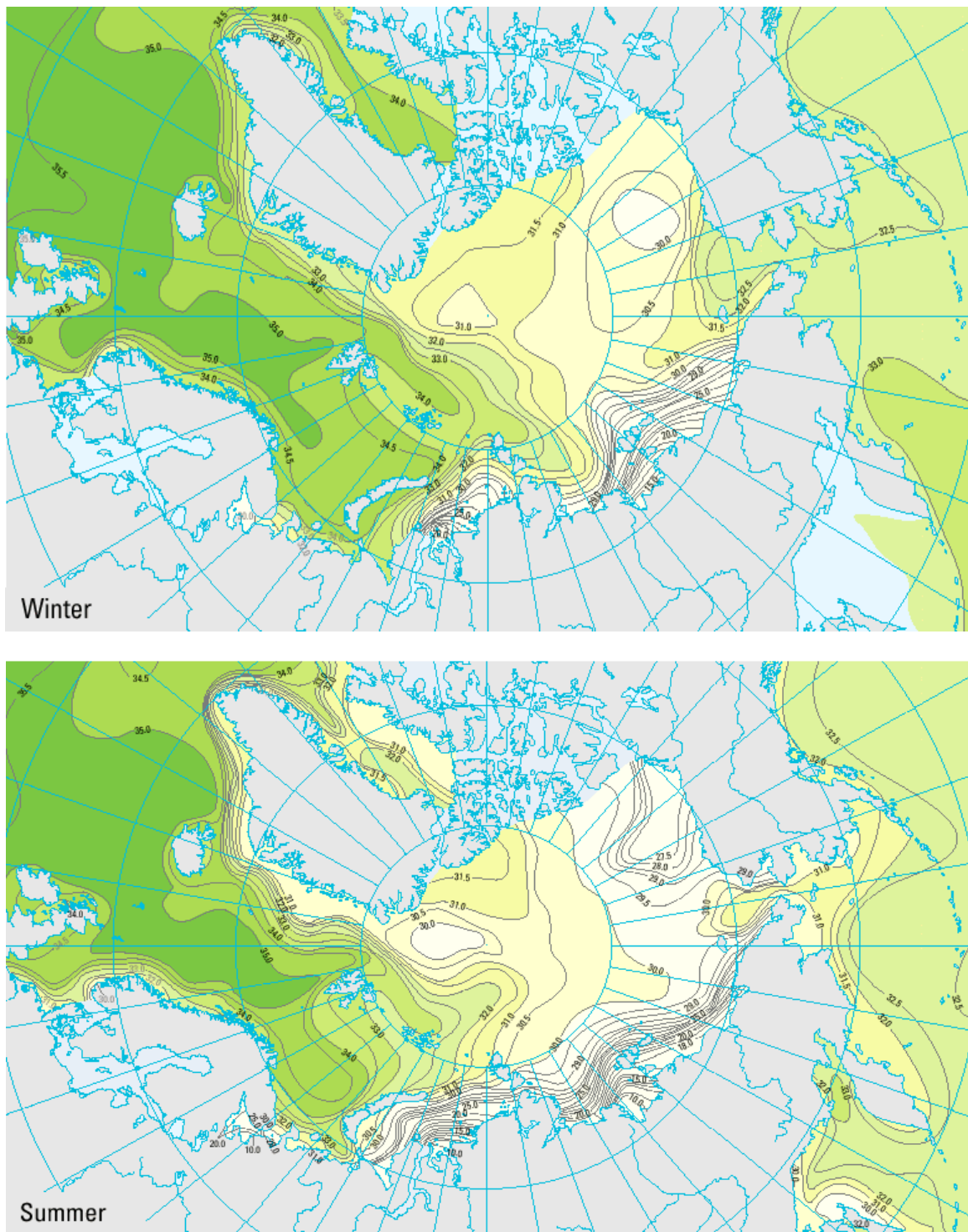


Figure 4. Winter and summer surface water salinity in the Arctic Ocean and adjacent seas (USSR Ministry of Defense 1980).

2. Circulation

The Arctic Ocean water mass can simply be described as waters comprised of relatively warm currents originating from the Atlantic and Pacific Oceans with cold outflow currents. Atlantic water enters the Arctic Ocean through Fram Strait and the Barents Sea, while a small percentage of Pacific water enters via Bering Strait. Water leaves the Arctic largely via Fram Strait, but also through the Canadian Arctic Archipelago (MacDonald and Bowers, 1996) (Figure 5). Most of the water in the Arctic Ocean originates from the Atlantic Ocean (79%). The inflow through the Bering Strait is a small percentage of the total (19%), but the relatively fresh surface water inflow contributes greatly to the stability and to the sea ice extent and distribution due to its stratifying effect.

The main water outflow is via the East Greenland Current (75%), the remaining outflow (25%) exits via the Canadian straits (25%) (AMAP Assessment Report, 1998).

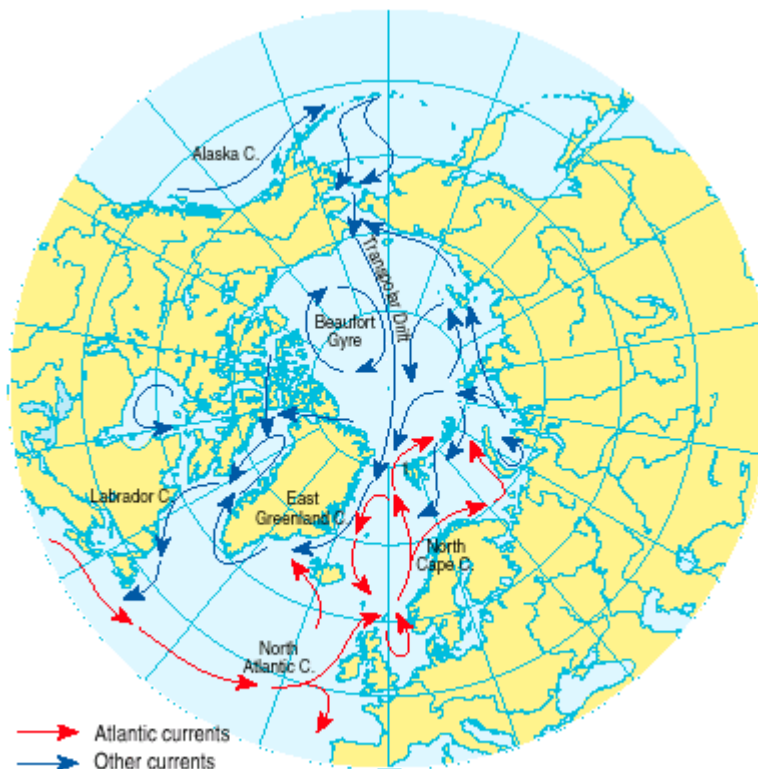


Figure 5. Surface ocean currents in the Arctic.

B. MIXED LAYER STRUCTURE

Differences in circulation and bathymetry between the Arctic Ocean and its marginal seas result in very different mixed layer structures. Of particular interest here is the contrast between the Beaufort and Chukchi Seas, located in the Western Arctic, and the Greenland Sea, a marginal sea located south of the Fram strait (Figure 2).

1. Beaufort and Chukchi Seas

The mixed layer structure in the Western Arctic is complex due to its topography of slopes, ridges and deep-sea plateaus. Here, waters from the Pacific and from the Atlantic meet forming two distinct water masses, separated by a cyclonic boundary current flowing along the Northwind Ridge (Figure 6). The overall impression of the Chukchi and Beaufort Seas is an ocean with considerable horizontal and vertical structure, and with a variable temperature and salinity profile. The Western Arctic region is highly stable due to the inflow and mixing of the buoyant fresh Pacific Water via the Bering Strait. The shallow Chukchi Sea is fed primarily by Pacific waters entering via the Bering Strait, which are modified and mixed with Beaufort Sea water in the interior of the Arctic Ocean along the Northwind Ridge, via canyons. The Barrow Canyon is a prime location for such interior mixing. The boundary current on the Northwind Ridge also acts as a source of interior Arctic waters for the Chukchi Sea during upwelling events near the shelf break (Woodgate et al, 2004). The Pacific inflow to the Arctic Ocean strongly contributes to stabilizing the upper ocean in the Western Arctic, thereby influencing ice thickness and upper-ocean mixing (Aagaard and Carmack, 1994). The inflowing Pacific water is less dense than the Arctic Ocean water due to its low salinity and higher temperatures compared to the cold Arctic Surface water. This creates a very fresh mixed layer, over a saline layer. Because salinity dominates the density profile the temperature excursions are less constrained by buoyancy forces (Figure 7). The impact of this weak and variable temperature profile is that thermohaline circulation does not provide a significant heat flux to the bottom of the ice in the Western Arctic (Woodgate et al, 2004).

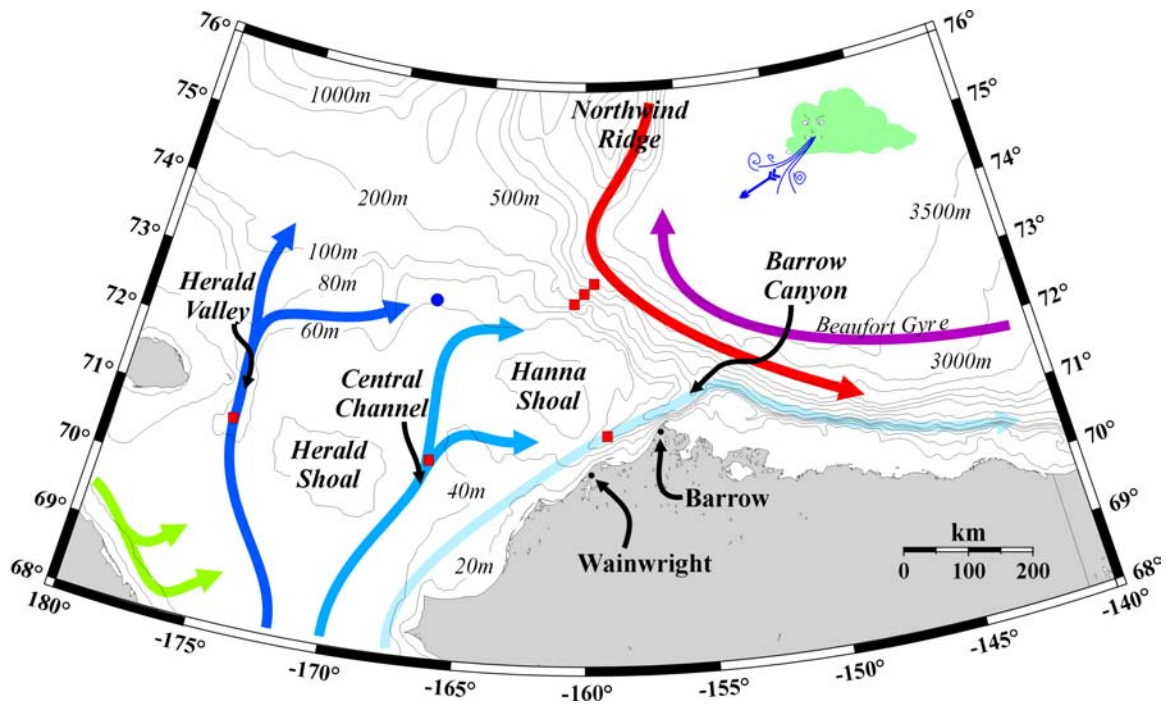


Figure 6. A schematic of the circulation over the Chukchi Sea and Beaufort/Chukchi slope (Weingartner, 2004)

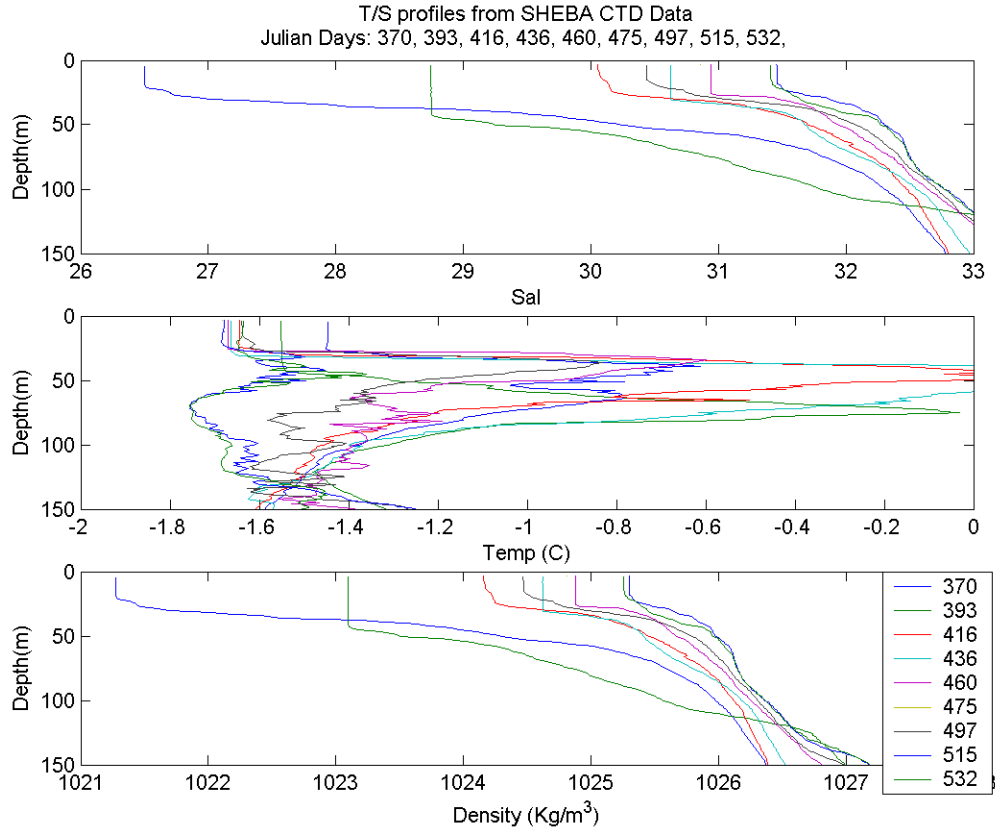


Figure 7. Beaufort and Chukchi Sea variable T/S profiles over the SHEBA study.

2. Greenland Sea

The circulation between the Atlantic and the Arctic Ocean results in a very different temperature and salinity profile in the Greenland Sea (Figure 8). The inflowing Atlantic water sinks as it enters the Arctic Ocean basin due to its high salinity compared to the cold but fresher Arctic Surface water. This Atlantic and Arctic water interaction creates a weaker salinity stratification and a stronger temperature inversion with depth compared to the Western Arctic (Figure 9). Because of this, the Greenland Sea thermohaline circulation readily responds to cooling and ice formation. It thus entrains a significant amount of heat from below and transfers heat to the atmosphere through leads, polynyas and seasonally open seas, allowing large surface heat fluxes. When ice is present, all of the heat entrained into the bottom of the mixed layer is fluxed upward to

melt the ice (Figure 10). Therefore the sea-ice-air exchanges coupled with the distinct ocean structure of the Greenland Sea promotes deep-water formation.

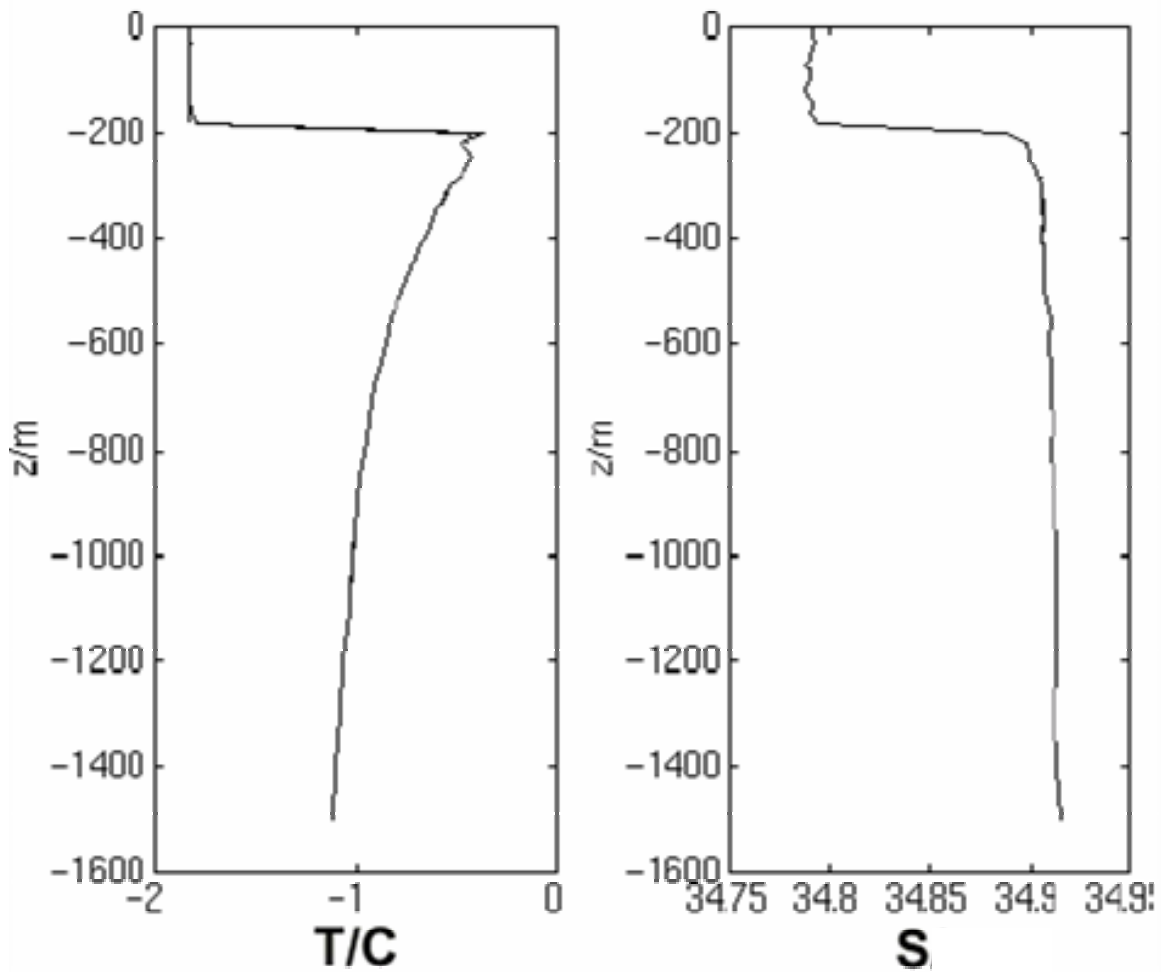


Figure 8. Representative Greenland Sea T-S profiles, from observations by Quadfasel and Ungewiß (1988)

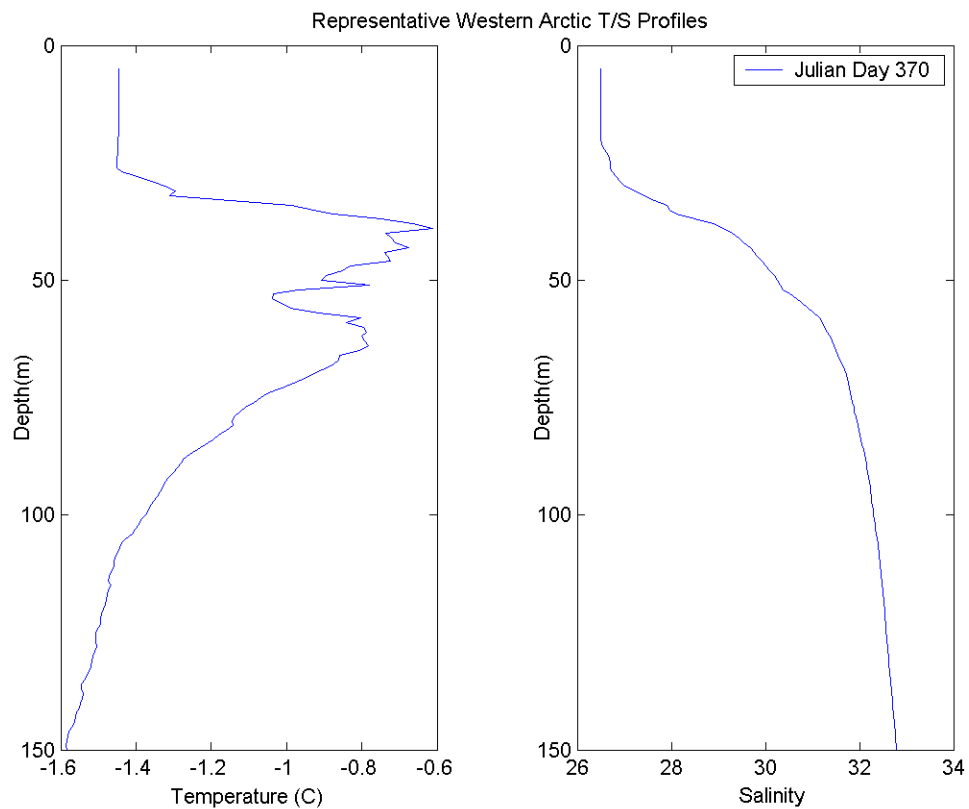


Figure 9. Western Arctic T/S profile comparison, from SHEBA (1997)

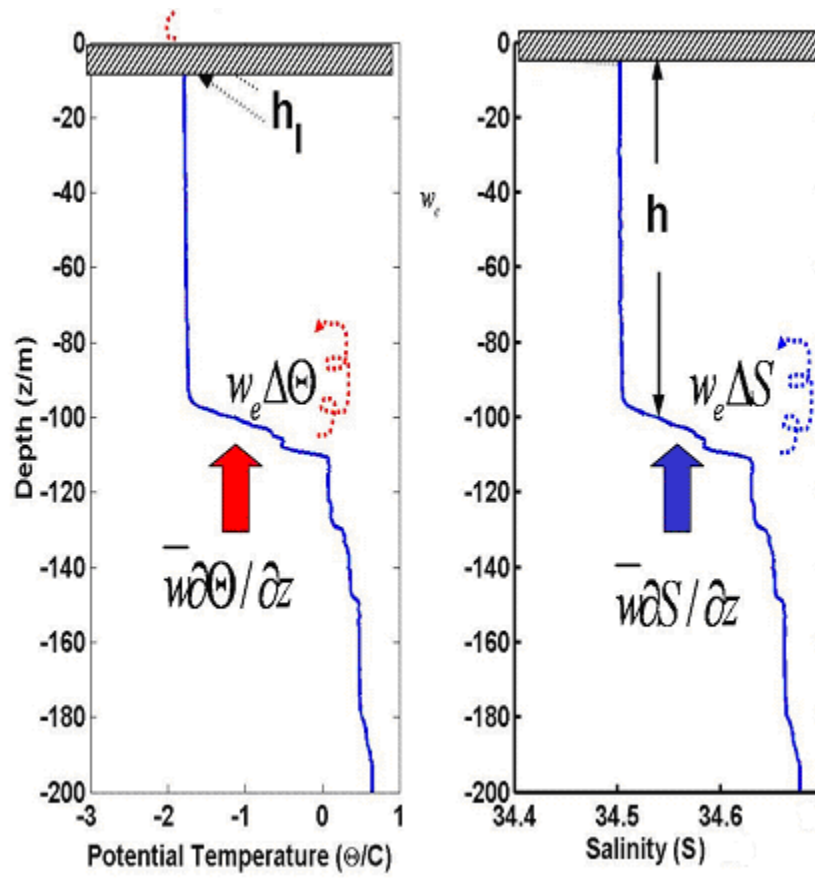


Figure 10. When ice is present all entrained heat is fluxed into the ice (Garwood, 2004).

C. DEEP CONVECTION

Deep convection in the polar seas plays a key role in the Earth's overall energy balance by exchanging heat stored in the ocean to the atmosphere. It is understood that strong atmospheric forcing, wind stress and surface cooling, must be present in conjunction with other conditions for deep convection to occur (Krauss and Businger, 1994). Strong winter cooling of northern surface waters along with brine rejection, as a result of ice formation, creates dense water at the surface that sinks and mixes with water from below. It causes heat to be transferred from the warmer ocean to the colder atmosphere or melt ice when present. Ideally, surface water must have a relatively high surface salinity so that the surface water will not freeze as it undergoes the intense cooling necessary in order to become dense enough to sink deeply. The integrated heat and salinity fluxes are vitally important components to this process because they determine the stability of the upper ocean. The short time scale wind stress and buoyancy fluxes are also important because they generate turbulent kinetic energy (TKE) that causes mixing and entrainment thereby deepening the mixed layer (Bramson, 1997).

In order to gain a better understanding of the important processes controlling deep convection, a comparison of a Western Arctic temperature and salinity profile and a Greenland Sea wintertime temperature and salinity profile will be used in conjunction with representative Arctic atmospheric forcing from SHEBA to illustrate the effects that varying temperature and salinity profiles have on deep convection under the same atmospheric forcing conditions.

1. Atmospheric Forcing

The pattern of mean sea-level pressure for January in the Arctic shows a low-pressure area over the North Atlantic Ocean around southern Greenland and Iceland (Icelandic Low) and a low-pressure area over the Pacific Ocean south of the Aleutians (Aleutian Low) (Figure 11). The influence of the Icelandic Low extends through the Fram Strait to the North Pole. Because of the Icelandic Low, the strongest winds occur in the Atlantic sector of the Arctic where they follow a track from Iceland to the Barents Sea. The Aleutian Low in the Pacific is blocked by the mountains of Alaska and northeast Siberia (Barry and Hare, 1974) and are weaker due to the influence of the high-pressure areas over central Canada and Tibet (AMAP Assessment Report, 1998).

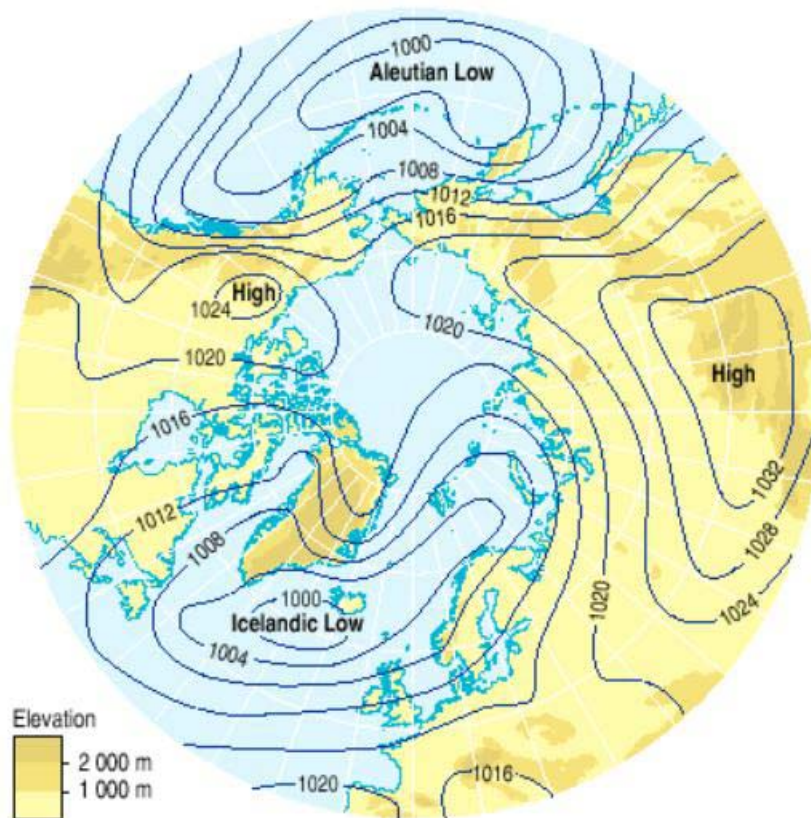


Figure 11. Mean sea-level pressure for January in the Arctic (AMAP Assessment Report, 1998)

In July, the winds weaken throughout the Arctic as the Aleutian Low disappears and the low-pressure area off Iceland shifts to southern Baffin Island in Canada (Canadian Low) (Figure 12) (AMAP Assessment Report, 1998).

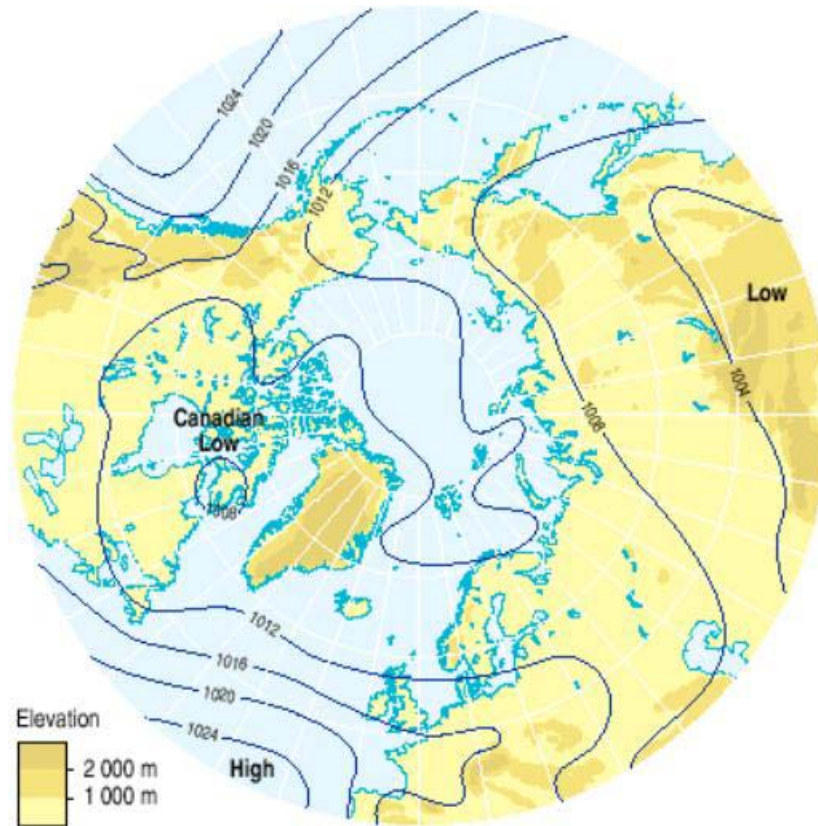


Figure 12. Mean sea-level pressure for July in the Arctic (AMAP Assessment Report, 1998).

D. NEAR SURFACE CONDITIONS AND OVERALL ENERGY BUDGET

Near-surface atmospheric pressure gradients and the attributed wind fields are primarily responsible for forcing the ice and ocean mixed layer circulation. As mentioned earlier, this stirring entrains heat the fluxes into the underside of the ice, resulting in melting. If the vertical circulation is weak compared to the stratification of the ocean then no heat will be entrained. Additionally, net solar radiation can act to induce melting or freezing. Melting ice introduces fresh water to the ocean mixed layer, creating negative salinity flux, and inhibiting entrainment. Conversely, ice formation increases the salinity at the surface of the mixed layer due to brine rejection, positive salinity flux, and enhances entrainment. The formation or melting of ice coupled with the mechanical mixing imparted by the wind stress along with the ocean density profile will

determine if and how much heat will be entrained and provided to the underside of the ice. Ultimately, ice will melt or freeze as a result of the overall energy balance.

1. SHEBA Atmospheric and Ice Measurement Data

Until recently, the polar region's atmospheric, and oceanographic processes have been poorly understood due to lack of year-round observations. Due to the short time-scale of the physical processes associated with sea-ice-air interactions, standard climate observations are inadequate for mixed layer modeling purposes. Measurements made at SHEBA provided the time-series data necessary for analyzing and understanding the synoptically and seasonally varying atmospheric and oceanic physical processes.

From October 1997 to October 1998, the SHEBA ice floe drifted more than 1400 km in the Beaufort and Chukchi Seas, with the latitude varying from 74°N to 81°N (Figure 13). The site was located in multiyear pack ice with summertime meltponds and occasional nearby leads.

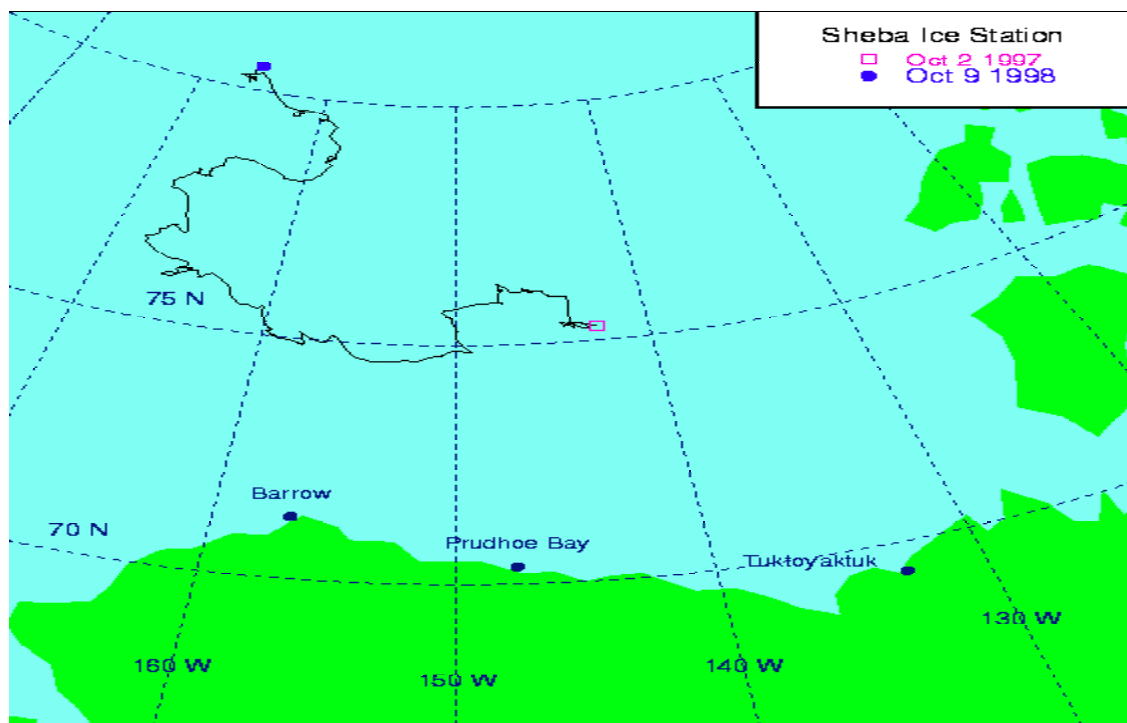


Figure 13. SHEBA ice floe drifted more than 1400 km in the Beaufort and Chukchi Seas (SHEBA Map of Ice Station Drift, 2004).

The drifting ice camp scientists (SHEBA Principal Investigators, 2004) made measurements of the atmospheric boundary layer, ice thickness and temperature and salinity profiles of the underlying ocean (Figure 14-16) (SHEBA Phase 2 Data Sets, 2004).

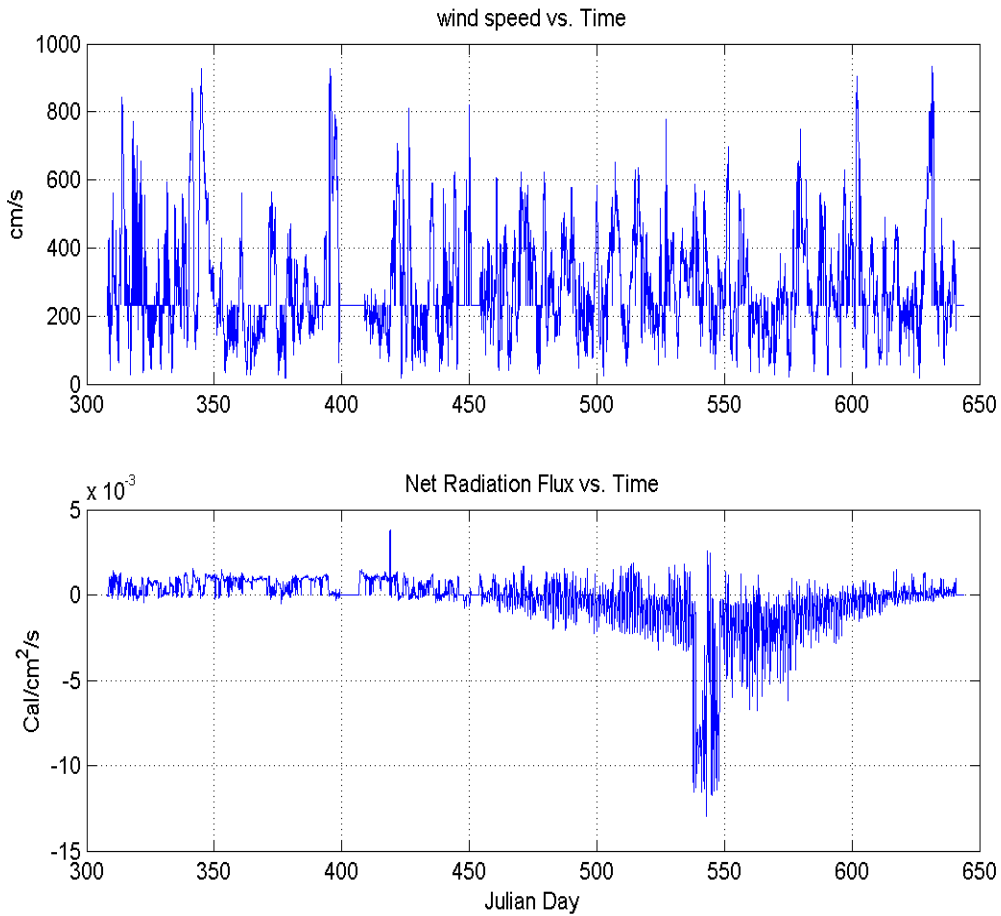


Figure 14. SHEBA atmospheric data

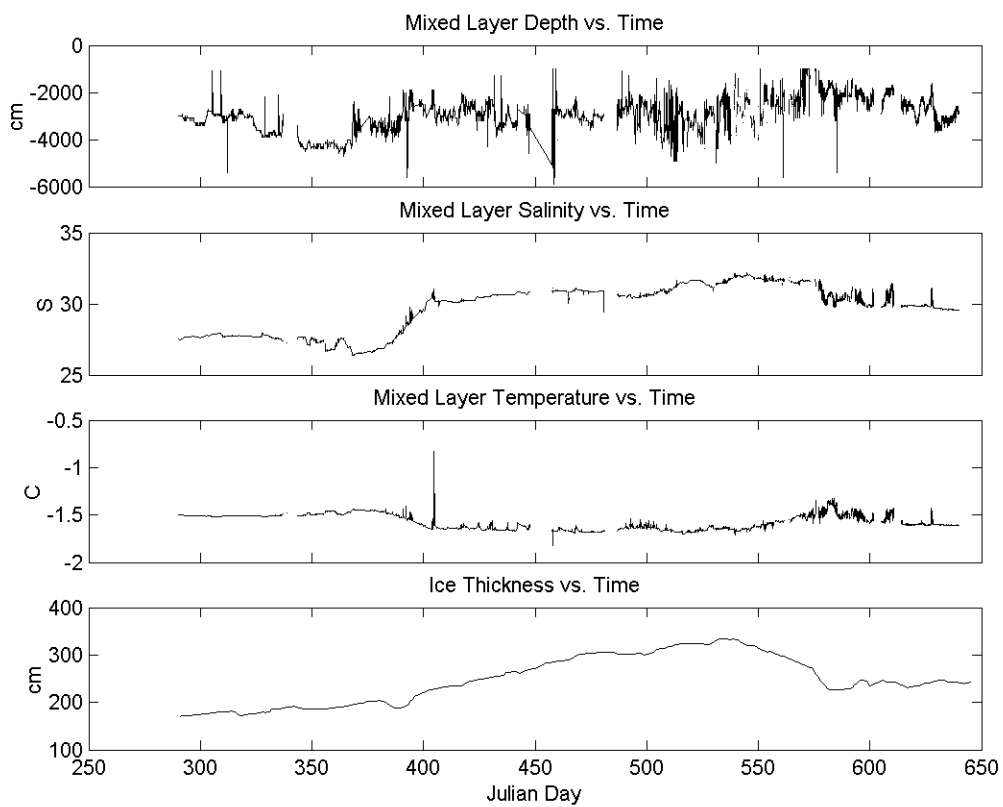


Figure 15. SHEBA ocean and ice measurement data

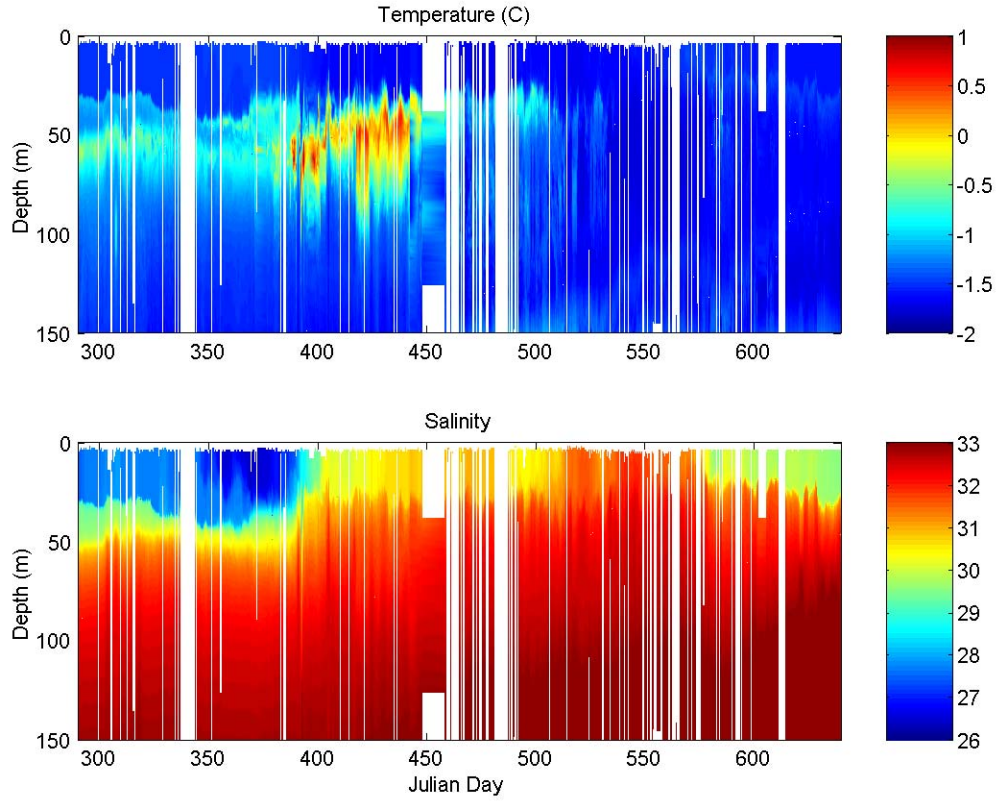


Figure 16. SHEBA temperature and salinity profiles of the ocean to 150 m.

a. Winds

The prevalent wind direction was from 40° to 120°, with the strongest winds between 800-900 cm/s. The strongest winds occurred in the winter and weakened during the summer months. Apparent seasonal changes in the winds recorded at the SHEBA site were probably due to a combination of the true seasonal wind signal and the significant change in geographic location due to the ice camp drift (Persson et al, 2002).

b. Total Energy Flux

The total energy flux, F_{tot} , into the surface is given by

$$F_{tot} = Q_0 - H_s - H_l + C \quad (1)$$

where C is the conductive flux, H_s is the sensible heat flux, H_l is the latent heat flux and Q_0 is the total net radiative flux given by

$$Q_0 = -Q_{si} + Q_{so} - Q_{li} + Q_{lo} \quad (2)$$

where Q_{si} is incoming shortwave radiation, Q_{li} is incoming longwave radiation, Q_{so} is outgoing shortwave radiation and Q_{lo} is outgoing longwave radiation. The assumption in (2) is that all radiative flux is absorbed within the ice. This is a good assumption considering our ice thickness is 200-400cm thick (Persson et al., 2002) .

For simplicity, the surface is considered as a slab of snow and ice (Figure 17). Therefore the conductive flux (C) is implicit in the radiative flux and F_{tot} becomes:

$$F_{tot} = Q_0 - H_s - H_l \quad (3)$$

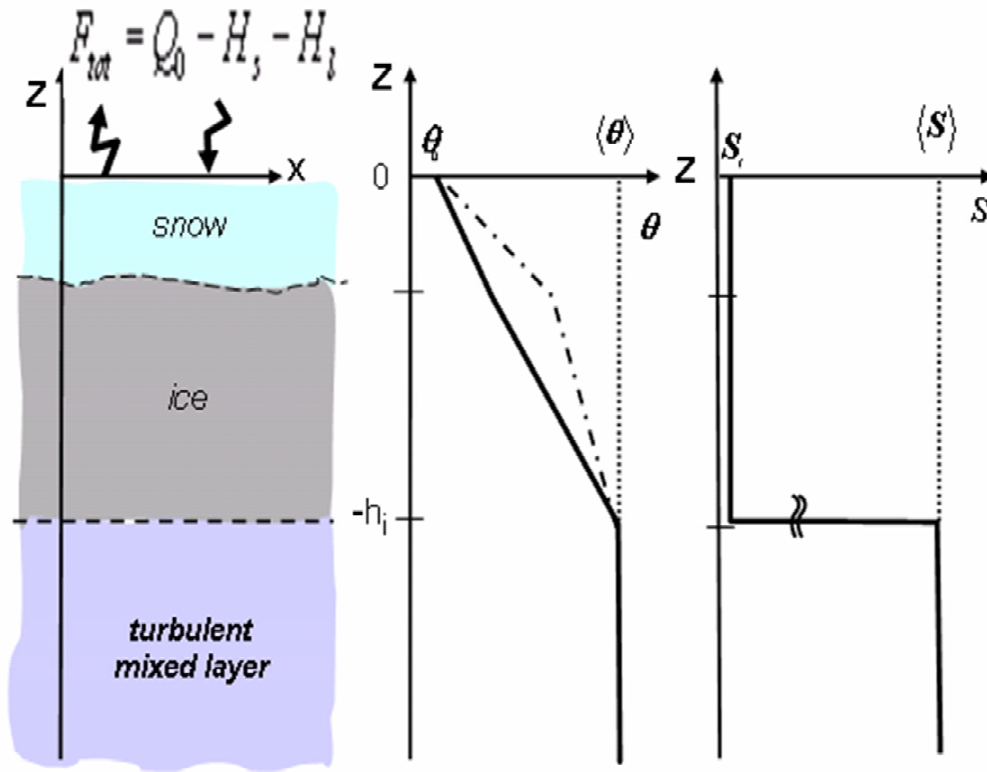


Figure 17. The surface is considered as a slab of snow and ice

Sensible heat flux, H_s , and latent heat flux, H_l , though small compared to the total net radiative flux Q_0 (Figure 18), are important because the sea-ice-air system is highly sensitive to small changes in the net heat flux due to the coupled nature of the system. The resulting sign convection is if F_{tot} is negative, the heat flux is into the ice. Thus the ice is gaining energy, which acts to melt the ice. If F_{tot} is positive this represents cooling and more ice will form.

The surface energy budget for SHEBA shows large day-to-day variability due to the large variability in the sensible and latent heat flux, shortwave and longwave radiation. In this case variations in the net solar radiation were due to cloud cover effects and albedo fluctuations due to changeable surface characteristics, i.e. fresh snow cover, white ice, and meltponds. The net shortwave radiation is negative from March to September, and the net longwave radiation is positive throughout the year. The magnitudes of sensible heat flux and latent heat flux are a factor of five to ten times smaller than the turbulent heat flux; warming the surface during the winter and weakly cooling during the summer time. Variability of sensible and latent heat flux is owed to the atmosphere vs. surface temperature gradients, which is affected by ocean feedback due to the presences of open water leads, and wind speed (Figure 19). Summing the radiation flux, sensible and latent heat flux yields a net heating from May through August and cooling for the period of September through March (Persson et al., 2002).

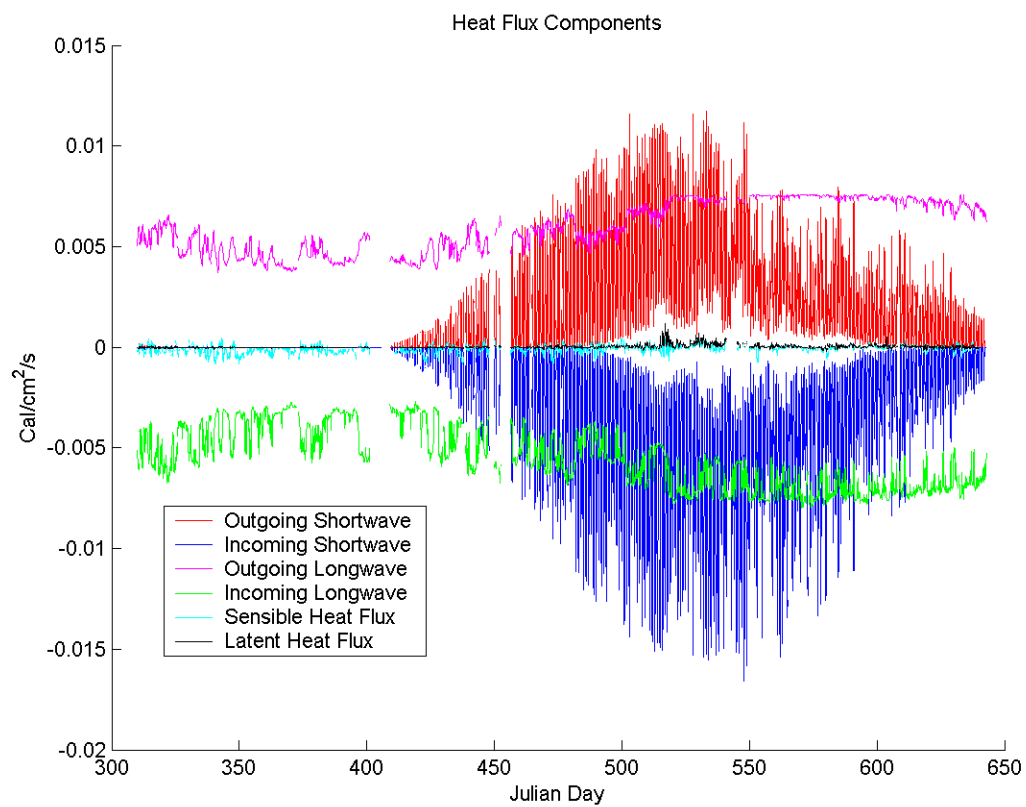


Figure 18. Heat Flux Components

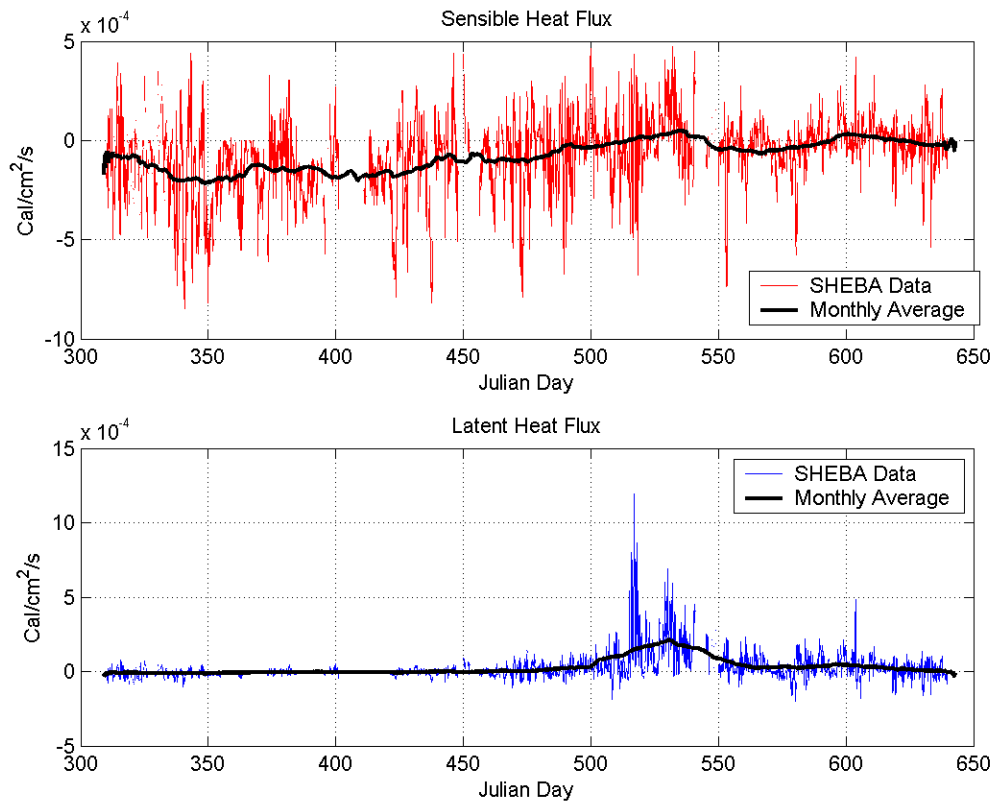


Figure 19. Sensible heat flux and latent heat flux warming the surface during the winter and weakly cooling during the summer time

c. Ice Thickness

The spatial and temporal evolution of sea ice is a combination of dynamic and thermodynamic processes. The observed thickness distribution is a result of the coupled mechanism of thermodynamic ice growth or melting and the compaction and dilation of the ice due to the dynamics of wind stress and ocean currents, which modify the spatial distribution of sea ice (Harder and Lemke, 1994). Daily estimates of the ice velocity, deformation, mean thickness, and thickness distribution were taken during the SHEBA experiment. From the start of the experiment in October to early mid June, 165 cm of ice formed. The summer melt season, lasting 52 days from June through August, resulted in 108 cm of ice melted. After this, ice formation continued; 17 cm was observed from early August to the conclusion of the experiment in October 1998. The data shows a net gain of 74 cm over a one-year period. This is not taken to be a result of

thermodynamic processes. It can probably be attributed to the change in geographic location due to the ice camp drift and dynamic processes such as convergence of the ice.

III. PROCEDURE

A. MIXED LAYER ICE COUPLE MODEL (MICE)

1. Ocean Mixed Layer Structure

The idealized ocean mixed layer is a homogeneous fully turbulent region of the upper ocean that is bounded above by the air-sea interface, and below by a turbulent entrainment zone. This entrainment zone is where temperature and salinity undergo dynamic instabilities, which give rise to entrainment fluxes of temperature and salinity. Below this entrainment zone is stratified water that increases in density with depth. The source of energy for the generation of turbulence in the mixed layer is provided by the fluxes of heat, salt and momentum at the sea-ice-air interface (Garwood, 1977).

2. Turbulent Kinetic Energy Budget

a. Notation

Seawater variables that vary in time and space may be decomposed into mean and fluctuating parts. For example, total potential temperature may be expressed as $\theta(x, y, z, t) = \bar{\theta}(z, t) + \theta'(x, y, z, t)$, where the overbar is a horizontal mean over a distance or horizontal model grid size L that is large compared with the scale of the fluctuations (turbulence integral scale), $\bar{\theta} = \frac{1}{L^2} \int \theta dx dy$. All mixed layer variables may be decomposed similarly into mean and turbulent parts, $T = \bar{T} + T'$, $S = \bar{S} + S'$, $u = \bar{u} + u'$, $v = \bar{v} + v'$, and $w = \bar{w} + w'$.

In addition to the horizontal mean, there is a vertical mean denoted by $\langle \rangle$

that is a vertical average over the mixed layer of depth h , $\langle \bar{\theta} \rangle = \frac{1}{h} \int_{-h}^{-h_i} \bar{\theta} dz$ between the bottom of the mixed layer, $z = -h$ and the bottom of the ice, $z = -h_i$.

Turbulent fluxes are associated with velocity-property covariances. For example, vertical heat flux is $\rho C_p \overline{\theta' w'}$ (Garwood, 2004).

b. Entrainment Hypothesis

The TKE budget is the basis for the entrainment hypothesis. The assumption is that turbulence contained within the mixed layer provides the energy needed to destabilize and erode the underlying stratified water mass. The amount of heat provided to the underside of the ice is dependent on this understanding of the dynamics of the mixed layer deepening or retreat (Garwood, 1977). The one-dimensional total TKE equation is:

$$\frac{\partial}{\partial t} \left(\frac{\overline{E}}{2} \right) = - \left[\overline{u'w'} \frac{\partial U}{\partial z} + \overline{v'w'} \frac{\partial V}{\partial z} \right] + \overline{b'w'} - \frac{\partial}{\partial z} \left[\overline{w' \left(\frac{u'^2 + v'^2 + w'^2}{2} + \frac{p'}{\rho_0} \right)} \right] - \varepsilon \approx 0 \quad (4)$$

where $\overline{E} = \overline{u'^2} + \overline{v'^2} + \overline{w'^2}$, u is the eastward velocity component, v is the northward velocity component, and w is the upward velocity component (z is positive up). To simplify the system of equations, horizontal homogeneity is assumed. The approximation of local homogeneity holds because of the short time scale for turbulence. Garwood (1977) recognized that the mean buoyancy and momentum fluxes are not one-dimensional for all time and space scales but effects such as advection are neglected in order to focus on new aspects of mixed layer modeling such a buoyancy flux enhancement. The terms of (4) are: time rate of change, shear production of horizontal TKE, buoyancy flux, transport of turbulence and viscous dissipation.

$$\frac{\partial}{\partial t} \left(\frac{\overline{E}}{2} \right) = \frac{\partial}{\partial t} \left(\frac{\overline{u'^2} + \overline{v'^2} + \overline{w'^2}}{2} \right): \text{Time rate of change or storage terms. In}$$

steady state these terms are equal to zero. These terms can be positive or negative but due to the rapid adjustment of turbulence they are assumed to be negligible compared to the production and dissipation terms.

$$- \left[\overline{u'w'} \frac{\partial U}{\partial z} + \overline{v'w'} \frac{\partial V}{\partial z} \right]: \text{Shear production of horizontal TKE. The}$$

production of forced convection due to wind stirring. This term can only be positive and is a large source of TKE.

$\overline{b'w'}$: Buoyancy Flux. This term can be positive or negative. When buoyancy flux is positive it is a source of vertical TKE. An unstable density profile will

result in free convection and positive buoyancy fluxes. However, if the oceanic profile is stable the buoyancy flux will damp the mechanical effects of the shear production and convert TKE to potential energy (PE).

$$-\frac{\partial}{\partial z} \left[\overline{w' \left(\frac{u'^2 + v'^2 + w'^2}{2} + \frac{p'}{\rho_0} \right)} \right] : \text{Transport of turbulence. Turbulence is}$$

advected when w' carries TKE or when fluid parcels collide passing one parcel's momentum and kinetic energy (KE) to the other. The advection and pressure transport terms do not change the total energy in the mixed layer they only move it around.

$\varepsilon = 3\varepsilon_{u'} = 3\varepsilon_{v'} = 3\varepsilon_{w'} : \text{Viscous Dissipation. This is a destruction term and can only be negative. At the small time and space scales the turbulence is isotropic. Therefore each of the different dissipation components is equal to each other and equal to one third of the total dissipation (Garwood, 1977).}$

c. *Integration of TKE*

Assuming steady state, and horizontal homogeneity the TKE budget (4) may be integrated from the bottom of the mixed layer, $z = -h$ to the bottom of the ice, $z = -h_i$.

$$\frac{\partial \langle \overline{E} \rangle h}{\partial t} = \int_{-h}^{-h_i} \left[\overline{u'w'} \frac{\partial U}{\partial z} + \overline{v'w'} \frac{\partial V}{\partial z} \right] dz + \int_{-h}^{-h_i} \overline{b'w'} dz - \int_{-h}^{-h_i} \varepsilon dz \quad (5)$$

The change in TKE in the mixed layer can be related to entrainment in terms of stratification and mixed layer depth, h . Stratification relates entrainment velocity and mean property jumps between the bottom of the mixed layer and the underlying layer to the vertical flux of the property out of the entrainment zone into the base of the mixed layer. Entrainment velocity can be described by the equation of mixed layer depth:

$$\frac{dh}{dt} = w_e - \overline{W} \Big|_{-h} \quad (6)$$

Assuming no vertical motion, $\overline{W} \Big|_{-h} = 0$, the equation becomes:

$$\frac{dh}{dt} = w_e \quad (7)$$

Wind stress at the surface produces turbulence in the surface layer this turbulence deepens the mixed layer mixing temperature, salinity, and momentum into the mixed layer.

$$\overline{\theta'w'} \Big|_{-h} = -w_e \Delta \bar{\theta} = \text{heat flux}$$

$$\overline{S'w'} \Big|_{-h} = -w_e \Delta \bar{S} = \text{salinity flux}$$

$$\overline{U'W'} \Big|_{-h} = -w_e \Delta \bar{U} = \text{momentum flux of eastward momentum.}$$

From this forced convection can be solved as a combination of the shear production at the surface and entrained momentum flux at the bottom of the mixed layer.

$$\int_{-h}^0 - \left[\overline{u'w'} \frac{\partial U}{\partial z} + \overline{v'w'} \frac{\partial V}{\partial z} \right] dz = 2m_3 u_*^3 + (\langle \bar{u} \rangle^2 + \langle \bar{v} \rangle^2) w_e \quad (8)$$

where u_*^3 is a wind forcing scale and m_3 is a shear production coefficient.

The buoyancy flux term can be expressed in terms of heat and salinity fluxes by the use of the linearized equation of state:

$$\rho = \rho_0 [1 - \alpha(\theta - \theta_0) + \beta(S - S_0)] \quad (9)$$

The buoyancy is defined as:

$$\overline{b'w'} = \alpha g \overline{\theta'w'} - \beta g \overline{S'w'} \quad (10)$$

where α is the thermal expansion coefficient and β is the salinity contraction coefficient.

Due to the pressure dependence of the thermal expansion coefficient buoyancy is not conserved. Unlike forced convection, buoyancy flux cannot be

expressed as a simple combination of the surface buoyancy flux and mixed layer buoyancy flux. The vertical integral of the buoyancy flux must be calculated (Garwood 1991). The thermal expansion coefficient varies with temperature, salinity and pressure, the thermobaric effect. This effect is small for shallow mixing but can be significant in deep mixing cases. The variation with depth is nearly linear (Figure 20).

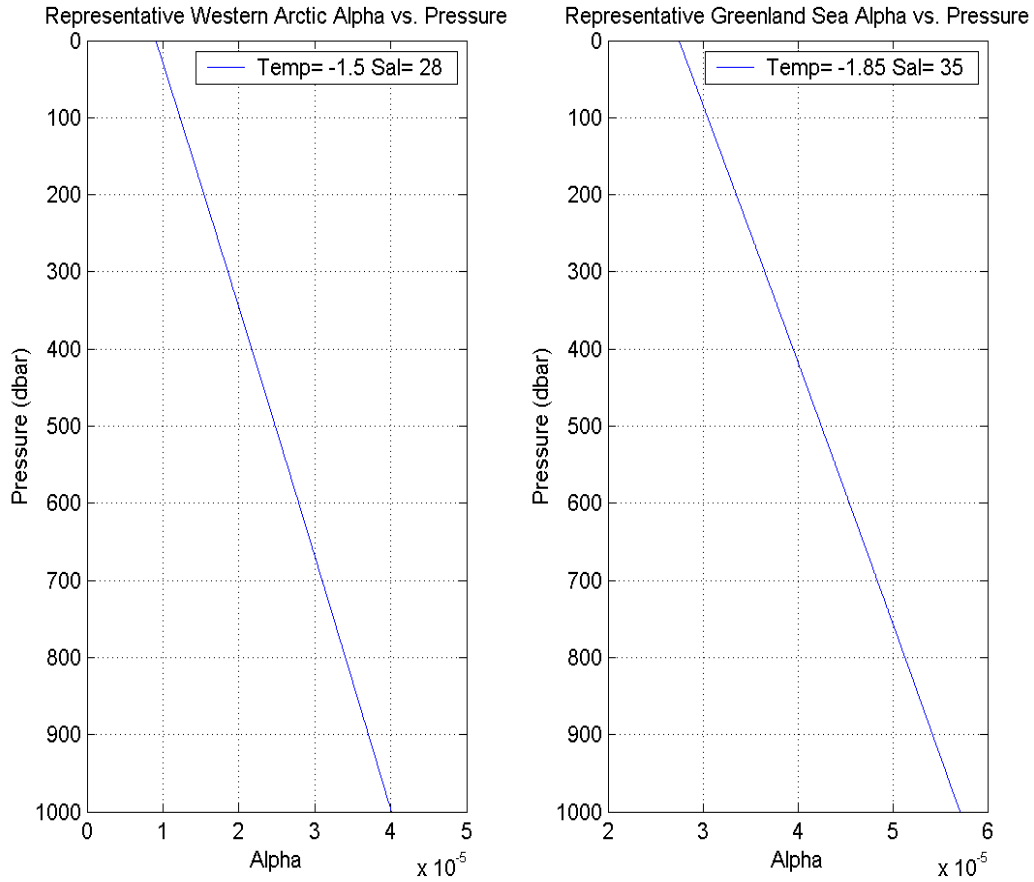


Figure 20. Linear variation of the thermal expansion coefficient with temperature, salinity and pressure

The thermal expansion coefficient can be written as:

$$\alpha \approx \alpha_0(\bar{\theta}, \bar{S}) - a_1(\bar{\theta}, \bar{S})z \quad (11)$$

where α_0 is the thermal expansion coefficient at the surface, and a_1 is a coefficient for the pressure enhancement of buoyancy. To add physical meaning to the

importance of the pressure enhancement of buoyancy flux Garwood (1991) defined a “thermobaric depth” at which the increased pressure doubles the thermal expansion coefficient relative to its surface value.

$$H_{\alpha} \approx \frac{\alpha_0}{a_1} \quad (12)$$

The thermobaric depth increases strongly with increasing potential temperature and weakly with increasing salinity (Figure 21).

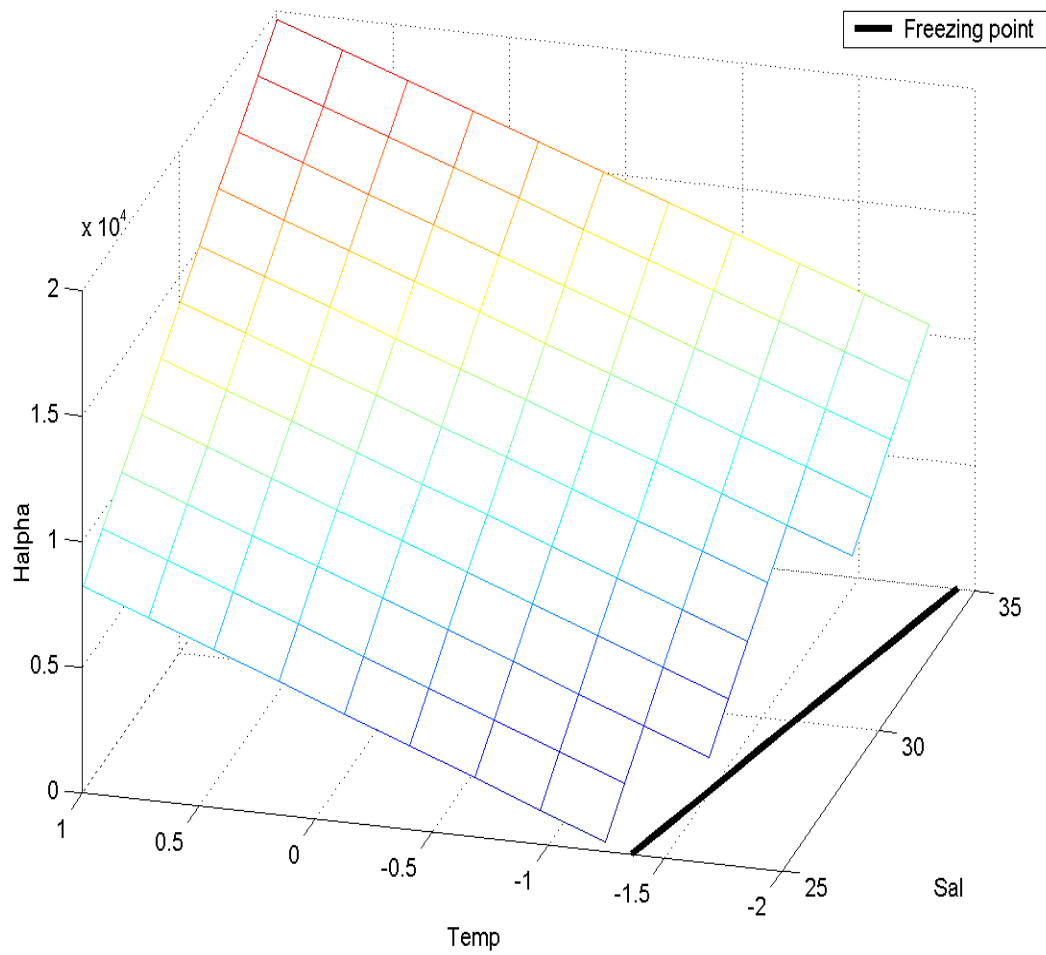


Figure 21. Dependence of H_{α} on potential temperature and salinity

Garwood (1991) defines a dimensionless depth of mixing as $\frac{h}{H_\alpha}$.

Buoyancy is conserved for $\frac{h}{H_\alpha} \ll 1$. In warmer ocean waters the thermobaric effect is negligible to depths of about 1000m. However, in cold polar oceans the dependence of α upon pressure cannot be neglected for mixing depths greater than 100m because of potential temperature's effect on the thermobaric depth (Garwood 1991).

In terms of thermobaric depth (12) the thermal expansion coefficient becomes:

$$\alpha = \alpha_o \left(1 - \frac{z}{H_\alpha} \right) \quad (13)$$

Buoyancy flux combined with equation (13) yields

$$\begin{aligned} \overline{b'w'} &= \overline{b'w'_\theta} - \overline{b'w'_s} \\ \overline{b'w'_\theta} &= \alpha_o \left(1 - \frac{z}{H_\alpha} \right) g \overline{\theta'w'} = \alpha g \left[\overline{\theta'w'_0} \left(1 + \frac{z}{h} \right) - \overline{\theta'w'_{-h}} \left(\frac{z}{h} \right) \right] \\ \overline{b'w'_s} &= \beta g \overline{S'w'} = \beta_o g \left[\overline{S'w'_0} \left(1 + \frac{z}{h} \right) - \overline{S'w'_{-h}} \left(\frac{z}{h} \right) \right] \end{aligned} \quad (14)$$

The vertical integral of buoyancy flux can now be solved for deep ocean mixing and polar seas cases.

$$\int_{-h}^0 \overline{b'w'}(z) dz = \int_{-h}^0 \left(\overline{b'w'_\theta} + \overline{b'w'_s} \right) dz$$

Taking the vertical integral of the potential temperature component of buoyancy flux, $\overline{b'w'_\theta}$:

$$\begin{aligned}
& \int_{-h}^0 \overline{b'w'_\theta} dz = \alpha_o g \int_{-h}^0 \left(1 - \frac{z}{H_\alpha}\right) \left[\overline{\theta'w'_0} \left(1 + \frac{z}{h}\right) - \overline{\theta'w'_{-h}} \left(\frac{z}{h}\right) \right] dz \\
& \overline{\theta'w'_0} = A \\
& \overline{\theta'w'_{-h}} = B \\
& = \alpha_o g \int_{-h}^0 \left(1 - \frac{z}{H_\alpha}\right) \left[A \left(1 + \frac{z}{h}\right) - B \left(\frac{z}{h}\right) \right] dz \\
& = \alpha_o g \int_{-h}^0 \left(1 - \frac{z}{H_\alpha}\right) \left[A + A \left(\frac{z}{h}\right) - B \left(\frac{z}{h}\right) \right] dz \\
& = \alpha_o g \int_{-h}^0 \left[\left(A + \left(\frac{Az}{h}\right) - \left(\frac{Bz}{h}\right) \right) - \left(\frac{Az}{H_\alpha} + \frac{Az^2}{hH_\alpha} - \frac{Bz^2}{hH_\alpha} \right) \right] dz \\
& = \alpha_o g \left[\left(Az + \frac{Az^2}{2h} - \frac{Bz^2}{2h} \right) - \left(\frac{Az^2}{2H_\alpha} + \frac{Az^3}{3hH_\alpha} - \frac{Bz^3}{3hH_\alpha} \right) \right] \\
& = \alpha_o g \left[(0 + Ah) + \left(0 - \frac{Ah}{2}\right) - \left(0 - \frac{Bh}{2}\right) - \left(0 - \frac{Ah^2}{2H_\alpha}\right) - \left(0 + \frac{Ah^2}{3H_\alpha}\right) + \left(0 + \frac{Bh^2}{3H_\alpha}\right) \right] \\
& = \alpha_o g \left[Ah - \frac{Ah}{2} + \frac{Bh}{2} + \frac{Ah^2}{2H_\alpha} - \frac{Ah^2}{3H_\alpha} + \frac{Bh^2}{3H_\alpha} \right] \\
& = \alpha_o g \left[\overline{\theta'w'_0}h - \frac{\overline{\theta'w'_0}h}{2} + \frac{\overline{\theta'w'_{-h}}h}{2} + \frac{\overline{\theta'w'_0}h^2}{2H_\alpha} - \frac{\overline{\theta'w'_0}h^2}{3H_\alpha} + \frac{\overline{\theta'w'_{-h}}h^2}{3H_\alpha} \right] \\
& = \alpha_o g \left[\overline{\theta'w'_0} \left(\frac{h}{2} + \frac{h^2}{6H_\alpha} \right) + \overline{\theta'w'_{-h}} \left(\frac{h}{2} + \frac{h^2}{3H_\alpha} \right) \right]
\end{aligned}$$

Vertical integral of the salinity component of buoyancy flux, $\overline{b'w'_s}$:

$$\begin{aligned}
\int_{-h}^0 \overline{b'w'_s} dz &= \beta_o g \int_{-h}^0 \left[\overline{S'w'_0} \left(1 + \frac{z}{h} \right) - \overline{S'w'_{-h}} \left(\frac{z}{h} \right) \right] dz \\
\overline{S'w'_0} &= C \\
\overline{S'w'_{-h}} &= D \\
&= \beta_o g \int_{-h}^0 \left[C \left(1 + \frac{z}{h} \right) - D \left(\frac{z}{h} \right) \right] dz \\
&= \beta_o g \int_{-h}^0 \left[C + \frac{Cz}{h} - \frac{Dz}{h} \right] dz \\
&= \beta_o g \left[Cz + \frac{Cz^2}{2h} - \frac{Dz^2}{2h} \right] \\
&= \beta_o g \left[(0 + Ch) + \left(0 - \frac{Ch}{2} \right) - \left(0 - \frac{Dh}{2} \right) \right] \\
&= \beta_o g \left[Ch - \frac{Ch}{2} + \frac{Dh}{2} \right] \\
&= \beta_o g \left[\overline{S'w'_0} h - \frac{\overline{S'w'_0} h}{2} + \frac{\overline{S'w'_{-h}} h}{2} \right] \\
&= \beta_o g \left[\frac{\overline{S'w'_0} h}{2} + \frac{\overline{S'w'_{-h}} h}{2} \right]
\end{aligned}$$

The resulting equation (15) illustrates the effect of the vertical integral of buoyancy flux, and its dependence on the vertical entrainment velocity. The potential temperature component of buoyancy flux is dependent on: surface temperature flux, temperature at the bottom of the mixed layer, mixed layer depth, and thermobaric depth. Since the haline contraction coefficient is not a function of pressure, the salinity component of buoyancy flux is only dependent on: surface salinity flux, (precipitation and evaporation with no ice present, melting and freezing when ice is present), salinity at the bottom of the mixed layer, and mixed layer depth.

$$\int_{-h}^0 \overline{b'w'}(z) dz = \alpha_o g \left[\overline{\theta'w'}_0 \left(\frac{h}{2} + \frac{h^2}{6H_\alpha} \right) + \overline{\theta'w'}_{-h} \left(\frac{h}{2} + \frac{h^2}{3H_\alpha} \right) \right] + \beta_o g \left[\overline{S'w'}_0 \left(\frac{h}{2} \right) + \overline{S'w'}_{-h} \left(\frac{h}{2} \right) \right] \quad (15)$$

3. 1-D Mixed Layer Ice Coupled Model

The Mixed layer-ICE coupled model (MICE) is a one-dimensional second-order turbulence closure solution for the first and second moments of the unsteady oceanic planetary boundary layer, including thermobaric enhancement of entrainment (Garwood, 1991). The MICE coupled model has ten prognostic equations obtained by integrating the mixed layer over the depth.

Mixed Layer Depth

$$\frac{dh}{dt} = w_e - \overline{W} \Big|_{-h} \quad (16)$$

Ice Thickness

$$\frac{dh_i}{dt} = F + Pr - Ev \quad (17)$$

When ice is present, precipitation, Pr, and evaporation, Ev, are zero. F, is the formation or melting of ice:

$$F = (Q_0 - \rho C_p \overline{\theta'W'} \Big|_{-h_i}) / (\rho_i L_i)$$

where Q_0 is the net upward surface heat flux, $Q_0 = Q_{Back}^{Radiation} + Q_{Sensible}^{Heat} + Q_{Latent}^{Heat} - Q_{Solar}^{Radiation}$, and $\overline{\theta'W'} \Big|_{-h_i}$ is the entrainment heat flux into the bottom of the ice from the ocean.

Integrated total TKE

$$d \frac{\langle \overline{E} \rangle h}{dt} = G_0 + G_h + \langle \overline{B'W'} \rangle h + D \quad (18)$$

is the sum of the vertically integrated shear production (8) and buoyancy flux (15), plus viscous dissipation, ε . An estimation of viscous dissipation can be made by taking the rate at which the largest eddies supply energy to the smaller eddies to be proportional to the reciprocal of the time scale of the largest eddies. The net rate of dissipation and the mean turbulent energy are used to define the dissipation time scale, τ_ε (Garwood, 1977).

$$\langle \varepsilon \rangle = \frac{\langle \overline{E} \rangle}{\tau_\varepsilon}$$

If the time scale of the largest eddy is proportional to the mixed layer depth divided by the rms turbulent velocity,

$$\tau = \frac{h}{\langle \overline{E} \rangle^{\frac{1}{2}}}$$

then,

$$D = \int_{-h}^0 \varepsilon dz = -2m_1 \langle \overline{E} \rangle^{3/2}$$

where m_1 is the dissipation coefficient.

Integrated vertical TKE equation is:

$$d \frac{\langle \overline{W'^2} \rangle h}{dt} = \langle \overline{B'W'} \rangle h + R_p + D/3 \quad (19)$$

where R_p is the redistribution of turbulent energy defined as:
 $R_p = 2m_2 \left(\langle \overline{E} \rangle - 3 \langle \overline{W'^2} \rangle \right) \langle \overline{E} \rangle^{1/2}$ (Lumley, 1974). The rational is that of a “return to isotropy”, meaning the pressure/strain interaction will tend to distribute equally energy among u, v, and w components.

The vertical integral of potential temperature flux from the base of the mixed layer to the sea-ice interface defines the change in mixed layer potential temperature

$$\frac{d\langle\bar{\theta}\rangle}{dt} = \frac{-\overline{\theta'W'}|_{-h_i} - \overline{\theta'W'}|_{-h}}{h} \quad (20)$$

Recall, $\overline{\theta'W'}|_{-h} = -w_e \Delta\bar{\theta}$. Thus the change in mixed layer salinity can be defined in the same way, or $\overline{S'W'}|_{-h} = -w_e \Delta\bar{S}$.

$$\frac{d\langle\bar{S}\rangle}{dt} = \frac{-\overline{S'W'}|_{-h_i} - \overline{S'W'}|_{-h}}{h} \quad (21)$$

The temperature flux at the top of the mixed layer

$$\overline{\theta'W'}|_{-h_i} = C_T C_D^{-1/2} \sqrt{E} \left(\langle\bar{\theta}\rangle - T_{fp} \right)$$

must be physical linked to the freezing point of the surface water, which is a function of the surface salinity flux, i.e. melting or freezing of ice.

$$\overline{SW'}|_{-h_i} = -F \left[\langle\bar{S}\rangle - S_i \right]$$

This interaction between temperature flux and salinity flux illustrates the strong coupling within the sea-ice-air system.

Mixed layer current and ice speed are calculated

$$d \frac{\langle\bar{U}\rangle h}{dt} = 2\Omega_Z \langle\bar{V}\rangle h + \frac{\tau_{ix}}{\rho} - \langle\bar{U}\rangle w_e - \frac{\langle\bar{U}\rangle h}{T_m} \quad (22)$$

$$d \frac{\langle\bar{V}\rangle h}{dt} = -2\Omega_Z \langle\bar{U}\rangle h + \frac{\tau_{iy}}{\rho} - \langle\bar{V}\rangle w_e - \frac{\langle\bar{V}\rangle h}{T_m} \quad (23)$$

$$d \frac{U_i h_i}{dt} = 2\Omega_Z V_i h_i + \frac{\tau_{0x}}{\rho_i} - \frac{\tau_{ix}}{\rho_i} - \frac{U_i h_i}{T_m} \quad (24)$$

$$d \frac{V_i h_i}{dt} = -2\Omega_Z U_i h_i + \frac{\tau_{0y}}{\rho_i} - \frac{\tau_{iy}}{\rho_i} - \frac{V_i h_i}{T_m} \quad (25)$$

where $\Omega_z = 7.29 \times 10^{-5} \sin(lat)$ is the Coriolis force. τ_{ix} is the atmospheric wind stress acting on the ice surface in the x-direction. τ_{0y} is the stress at the sea-ice interface acting on the ocean surface in the y-direction. T_m is a damping term to dissipate energy within the system.

The entrainment velocity is calculated by vertically integrating the TKE budget (Bramson, 1997), giving:

$$w_e = \left\langle \overline{W'^2} \right\rangle^{1/2} \left\langle \overline{E} \right\rangle / \left(h \Delta \bar{B} + \left\langle \overline{E} \right\rangle \right)$$

This gives a system of ten prognostic equations: mixed layer depth, (26), ice thickness, (27), total TKE, (28), vertical TKE, (29), mixed layer potential temperature, (30), mixed layer salinity, (31), mixed layer velocity components, (32) and (33), and ice velocity components, (34) and (35); for a sea-ice-air mixed layer model that can be solved.

THIS PAGE INTENTIONALLY LEFT BLANK

IV. SENSITIVITY STUDIES

The following sensitivity studies demonstrate the strongly coupled feedback system for sea-ice-air interactions in the high latitudes. Realistic high arctic synoptic forcing, provided by SHEBA wind and net radiation fluxes, were used to examine the effects of MICE model's sensitivity to varying initial conditions. Initial conditions include: turbulent kinetic energy, mixed layer depth, and temperature and salinity profiles.

Representative Western Arctic and Greenland Sea profiles were used to demonstrate how important realistic ocean structure is to forced convection, free convection and total TKE. The dependence of ice melting or formation on the magnitude of wind speed was studied by varying wind forcing by 50% to 100% of the observed forcing with the same surface cooling and same Greenland Sea temperature and salinity profile. The effect of the net heat flux was studied by running simulations with heat flux values that were about $\pm 0.0002 \text{ cal cm}^{-2} \text{ s}^{-1}$ of the observed forcing, with the same wind forcing and same Greenland Sea temperature and salinity profiles. The decrease or increase in net heat flux was representative of the warming attributable to the increased sensible heating due the presence of warmer air aloft or cooling effects attributable to latent heat cooling due to the presence of leads. Finally, a moving average was applied to the atmospheric forcing to simulate daily, weekly and monthly forcing. The simulated daily, weekly, and monthly atmospheric data along with the measured hourly data was used to examine the effects on the MICE model's skill due to the varying time scales of the forcing data.

The values for the physical constants are given in Table 1 and surface boundary, and below-layer forcing conditions for the Western Arctic and Greenland Sea are given in Table 2.

Description	Symbol	C-G-S Value
Freezing Temperature	T_{fp}	Function of Salinity
Surface thermal expansion coeff.	α_0	$7.44 \times 10^{-6} \text{C}^{-1}$
Thermobaric depth	H_α	215220 cm
Haline contraction	β_0	7.94×10^{-4}
Ice salinity	S_i	6 psu
Representative seawater density	ρ	1.028 gm/cm^3
Ice density	ρ_i	0.905 gm/cm^3
Representative air density	ρ_a	$.00125 \text{ gm/cm}^3$
Latent heat of fusion for seawater	L_i	66.88 cal/gm
Heat capacity of seawater	C_p	0.9297 cal/gm/C
Ice thermal conductivity	λ_i	0.0048 cal/s/cm/C
Drag/heat transfer coefficients	$C_D = C_T$	1.5×10^{-3}
Planetary rotation	Ω_z	$1.4 \times 10^{-4} \text{s}^{-1}$
Dissipation coeff.	m_1	1
Pressure Redistribution. coeff.	m_2	0.5
Shear Production coeff.	m_3	6
Damping Coefficient	T_m	8640 s

Table 1. Table of Values for Physical Constants.

Description	Symbol	C-G-S Value
Surface heat flux	Q_0	SHEBA Measured Data (Cal/cm ² /s)
Eastward wind stress	τ_x	Calculated (dyn/cm ²)
Northward wind stress	τ_y	Calculated (dyn/cm ²)
Vertical Mean Velocity at bottom of mixed layer	\overline{W}_{-h}	0 cm/s
Western Arctic Temperature just below mixed layer	$\overline{\theta}_{below}$	-1.07 C
Western Arctic Salinity just below mixed layer	\overline{S}_{below}	29.31
Greenland Sea Temperature just below mixed layer	$\overline{\theta}_{below}$	-0.33 C
Greenland Sea Salinity just below mixed layer	\overline{S}_{below}	34.88

Table 2. Table of Surface Boundary and Below-Layer Forcing Conditions .

A. VARYING INITIAL CONDITIONS

1. Turbulent Kinetic Energy

Sensitivity to varying initial TKE was examined by running the MICE Model with purposefully too-high, reasonable, and too-low initial TKE values. For the Greenland Sea case values of 0.1 cm²/s², 0.3 cm²/s² and 1.0 cm²/s², for low, best guess and high values respectively were used (Figure 22-23). Examining the resulting plots of TKE shows the TKE converging quickly to a balanced solution. The model achieves a good solution within 10 hours, and the TKE solution is fully spun up by 0.5 day and does not diverge throughout the model run.

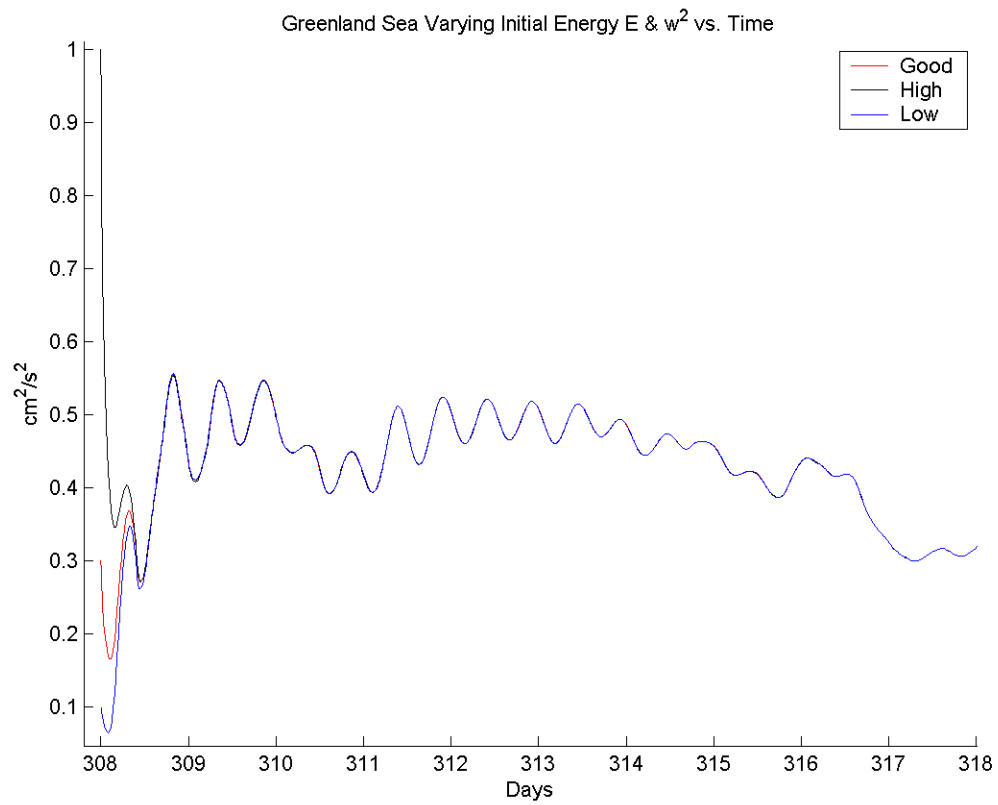


Figure 22. Sensitivity to varying TKE - Greenland Sea Julian Day 308-318.

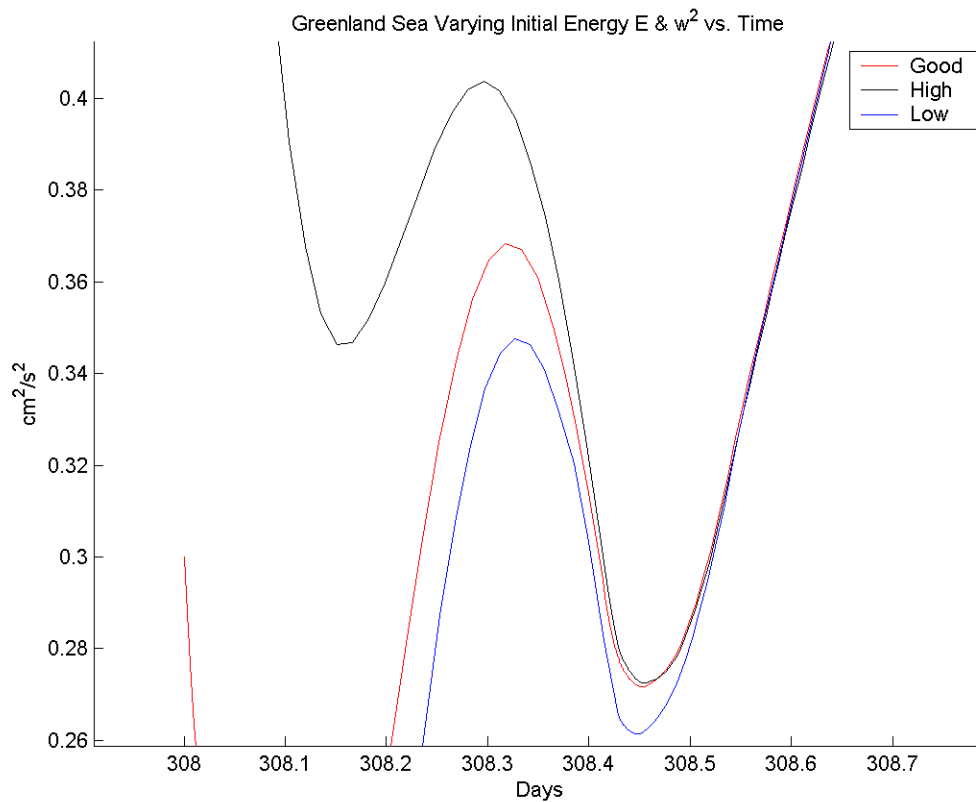


Figure 23. TKE Convergence at 0.5 Day- Greenland Sea Julian Day 308-318.

2. Mixed Layer Depth, Temperature and Salinity Profile

Western Arctic and Greenland Sea profiles were run using the same representative synoptic forcing to illustrate the effect of the initial underlying ocean structure on ice melting and/or formation. Both cases were run under relatively light wind conditions where the circulation was primarily thermally driven due to surface cooling and ice freezing. The Western Arctic initial mixed layer depth was 2800 cm, initial mixed layer temperature was -1.51 C and initial mixed layer salinity was 27.75. The Greenland Sea initial mixed layer depth was 199 m. Initial mixed layer temperature was -1.91 C, based on the freezing point at the initial mixed layer salinity of 34.79. Figure 24 is a comparison of the two different initial profiles.

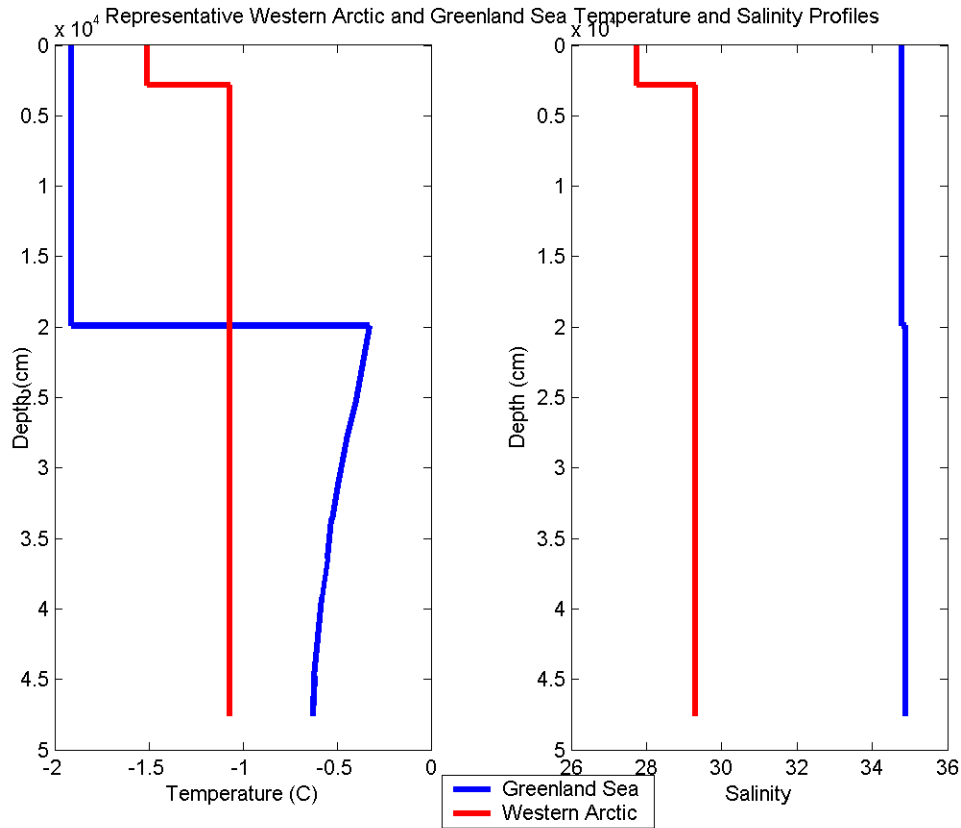


Figure 24. Representative Ocean Structure for Western Arctic and Greenland Sea.

The Greenland Sea has weaker salinity stratification and a stronger temperature inversion than does the Western Arctic. Therefore, by the entrainment hypothesis, we would expect more mixing. The results show this to be the case (Figure 25). During the fifty day MICE model run the representative Greenland Sea mixed layer deepens 2000 cm whereas the representative Western Arctic mixed layer deepens 500 cm.

Due to the net surface cooling there is ice freezing in both cases, but the greater entrained heat into the ice from the underlying ocean in the Greenland Sea profile results in less ice formation. The Greenland Sea forms 5.5 cm of ice during the fifty day run. Under the same atmospheric conditions the Western Arctic forms 35.5 cm. The salinity increase of 0.51 is associated with the physical process of brine rejection due to ice freezing. As the salinity increases, the freezing point decreases. Figure 26 shows heat

storage for both the Greenland Sea and Western Arctic mixed layer. Physically, the ice is acting as an insulating cap that does not allow entrained heat to directly escape to the atmosphere. Recalling the prognostic equation for the mixed layer temperature is $\frac{d\langle\bar{\theta}\rangle}{dt} = \frac{-\bar{\theta}'W'|_{-h_i} - \Delta\bar{\theta}w_e}{h}$, the MICE model allows of this for the heat storage by regulating the heat flux into the ice. The temperature flux at the top of the mixed layer is $\bar{\theta}'W'|_{-h_i} = C_T C_D^{-1/2} \sqrt{E} (\langle\bar{\theta}\rangle - T_{fp})$, where $\langle\bar{\theta}\rangle - T_{fp}$ is the difference of mixed layer temperature from the freezing point. Fluctuations in this temperature difference are an order of magnitude smaller than the fluctuations in TKE. The square root of Total TKE present in the system, \sqrt{E} , governs the transfer of heat into the ice and thereby heat storage in the mixed layer (Figure 27).

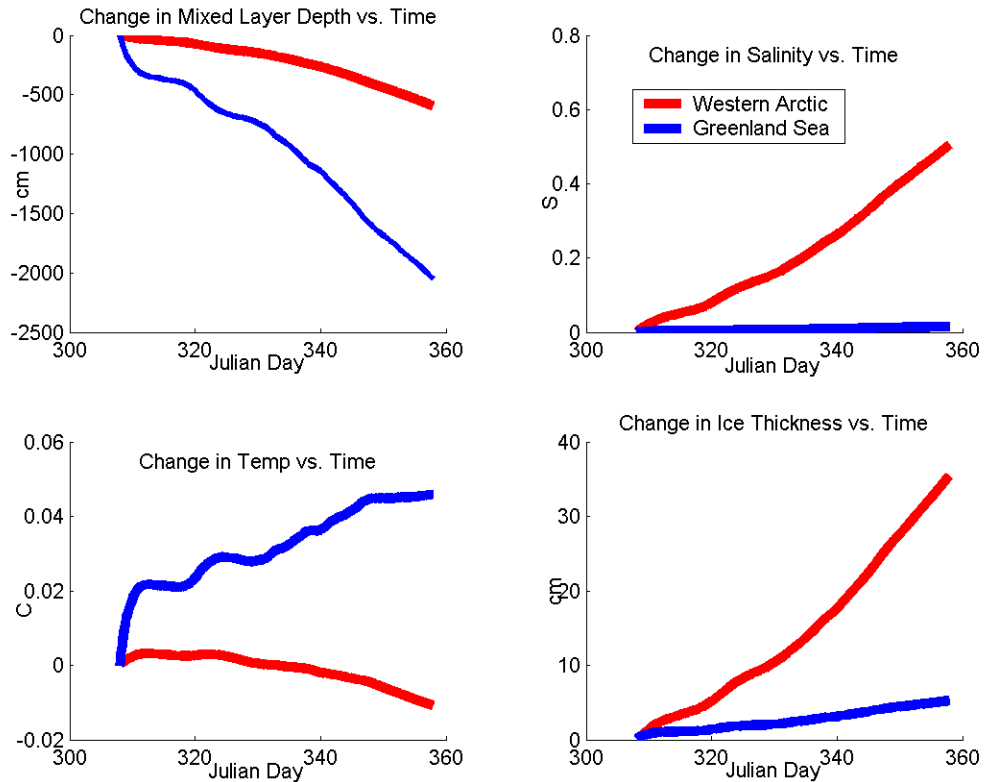


Figure 25. Sensitivity to Initial conditions: h , $T(z)$, $S(z)$.

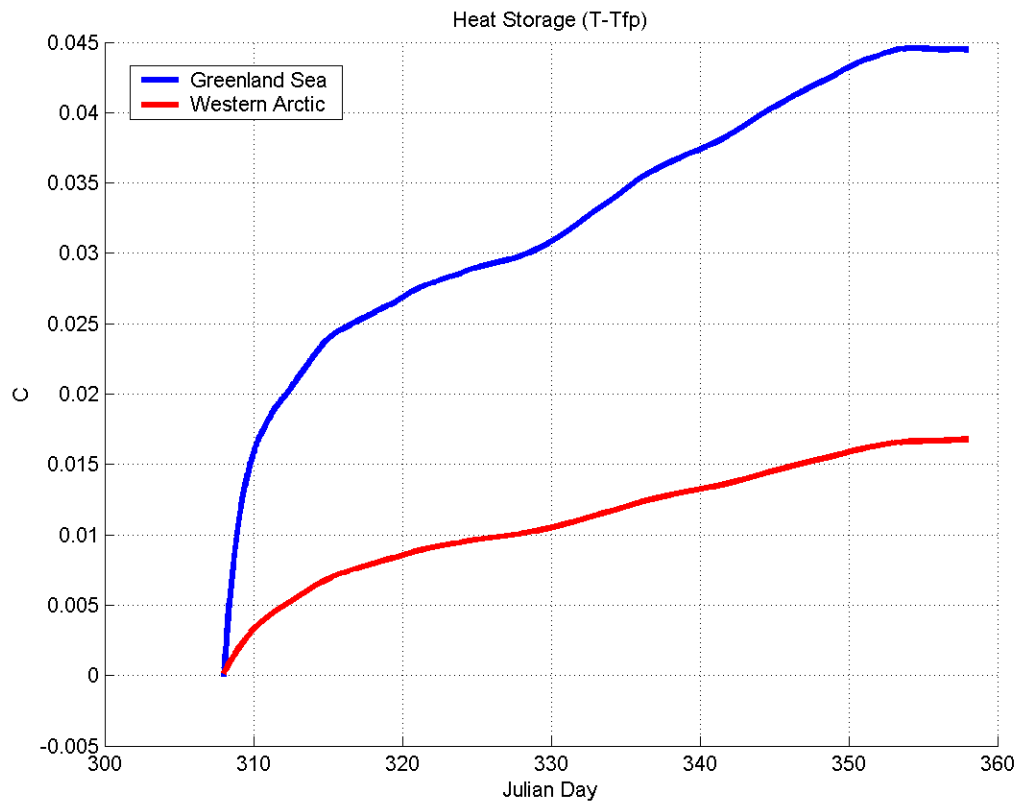


Figure 26. Heat storage for both the Greenland Sea and Western Arctic mixed layer.

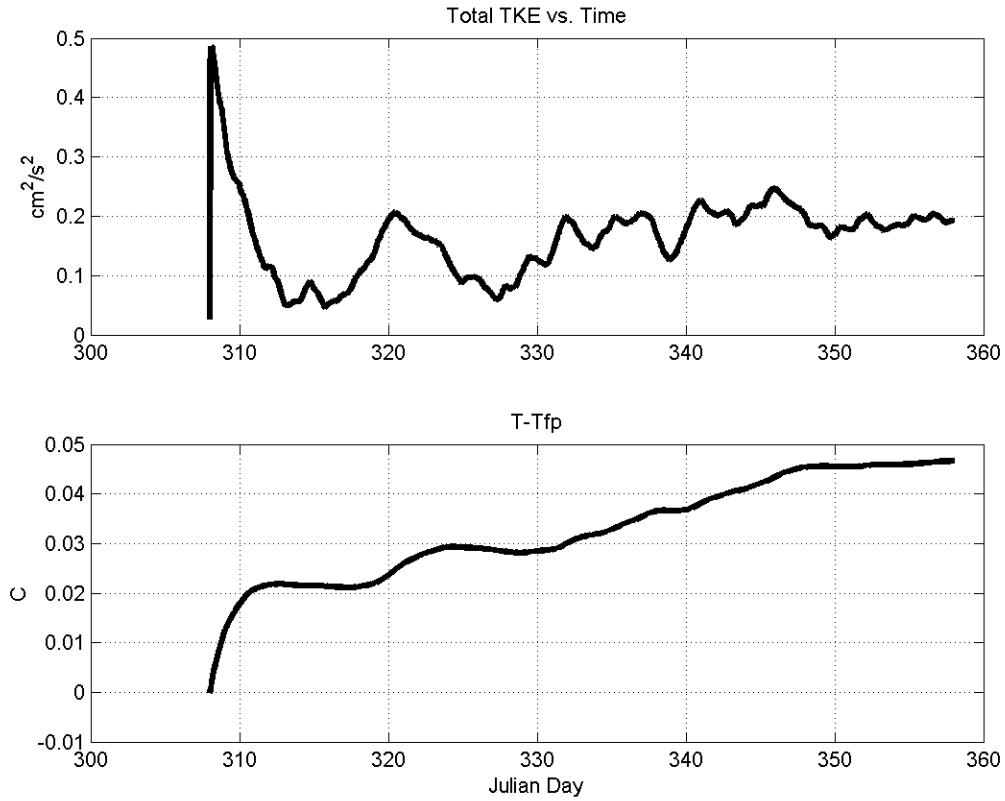


Figure 27. Difference of mixed layer temperature from the freezing point is an order of magnitude smaller than the TKE in the system

B. VARYING WIND SPEED WITH THE SAME NET HEAT FLUX

The dependence of melting and freezing on wind speed was examined by running three different wind forcing cases with the Greenland Sea temperature and salinity profiles (Figure 24) for thirty days. The SHEBA representative synoptic wind timeseries (Figure 14) was used for case 1. As a control, the SHEBA winds were applied to the Greenland Sea case in order to isolate the dependence upon initial ocean conditions using realistic synoptically varying winds. Case 2 the same wind was increased 50% and for case 3 the wind forcing was increased 100%.

The results illustrate the complex and coupled nature of the sea-ice-air system (Figure 28). The system melts and freezes ice in pulses, with significant negative feedback tied in with the periods of rapid entrainment. Generally the deepening mixed layer entrains heat, which increases the mixed layer temperature and heat storage. Then

the extra heat contained in the mixed layer is transferred to the underside of the ice in proportion to the square root of total TKE present in the system, \sqrt{E} . At the same time the salinity fluxes due to ice melting and formation impact the buoyancy flux which has a direct effect on the entrainment.

The mixed layer depth plot (Figure 28) shows slightly greater deepening for the lowest wind case and the least deepening for the highest wind speed case. This result is due to the effect on free convection of the salinity flux from ice melting. The melting ice creates a positive salinity flux, $\overline{SW'}|_{-h_i} = -F[\langle\bar{S}\rangle - S_i]$ at the top of the mixed layer, which in turn damps the free convection by inducing a negative buoyancy flux,

$$\langle\overline{B'W'}\rangle h = \alpha_0 g h \left[\left(1 + \frac{h}{3H_\alpha}\right) \overline{\theta'W'}|_{-h_i} - \left(1 + \frac{2h}{3H_\alpha}\right) \Delta\bar{\theta}_{w_e} \right] - \beta_0 g h \left[\overline{S'W'}|_{-h_i} - \Delta\bar{S}_{w_e} \right].$$

The degree to which buoyant damping or enhancement is occurring is very complex because simultaneously the increasing wind is providing more heat to the ice bottom due to the increased TKE (Figure 29). The greater heat to the ice bottom is apparent in the change in ice thickness between the three cases. Case 1 and case 2 show a modest ice formation of 1.22 cm and 0.55 cm respectively. However the highest wind case, case 3, resulted in 0.17 cm of ice melting despite the smallest entrainment values. Due to the increased TKE of the highest winds, the heat storage in the mixed layer was less, and more heat was transferred into the ice bottom from the underlying ocean. Figure 30 shows the high frequency fluctuations at which ice melting or freezing will occur. Ice freezing is based on the net atmosphere and ocean inputs. Heat is lost to or gained, from the atmosphere and heat lost to or gained, from the ocean. Ice losing heat to the ocean seems unphysical but if the freezing point of seawater is less than the temperature of the ice, the ice can give up heat to the water. $F = (Q_0 - \rho C_p \overline{\theta'W'}|_{-h_i}) / (\rho_i L_i)$. If heat is lost, more ice will form. If heat is gained, the ice will melt.

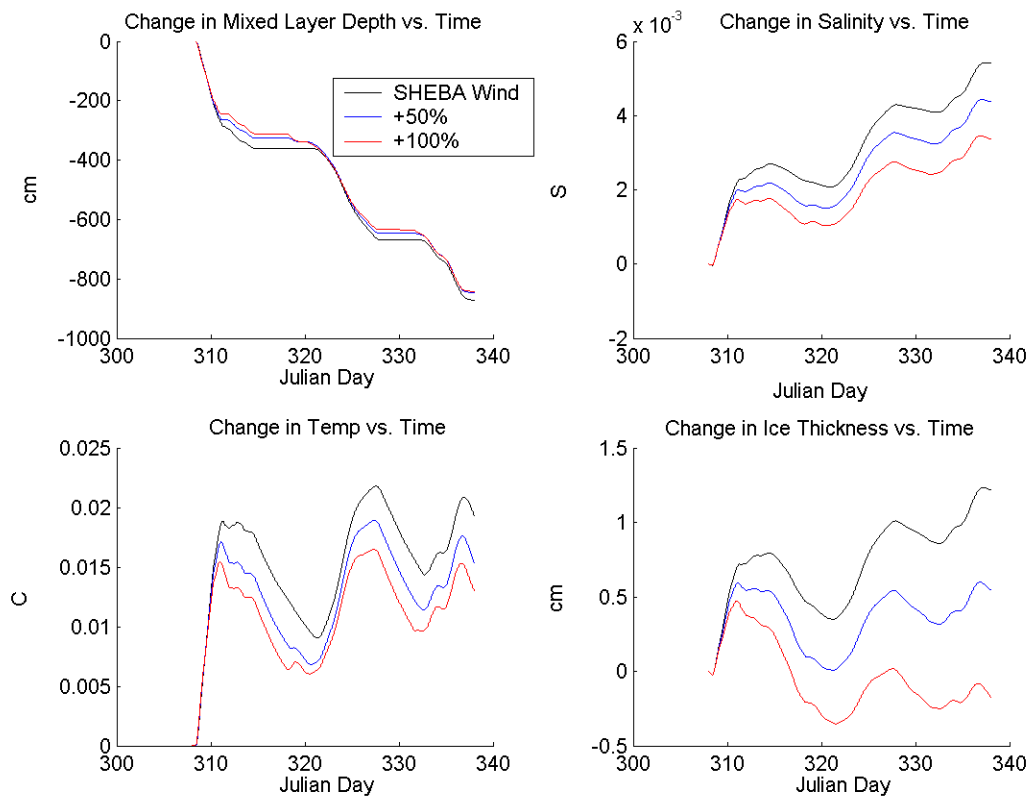


Figure 28. Varying Wind Speed same Net Heat Flux

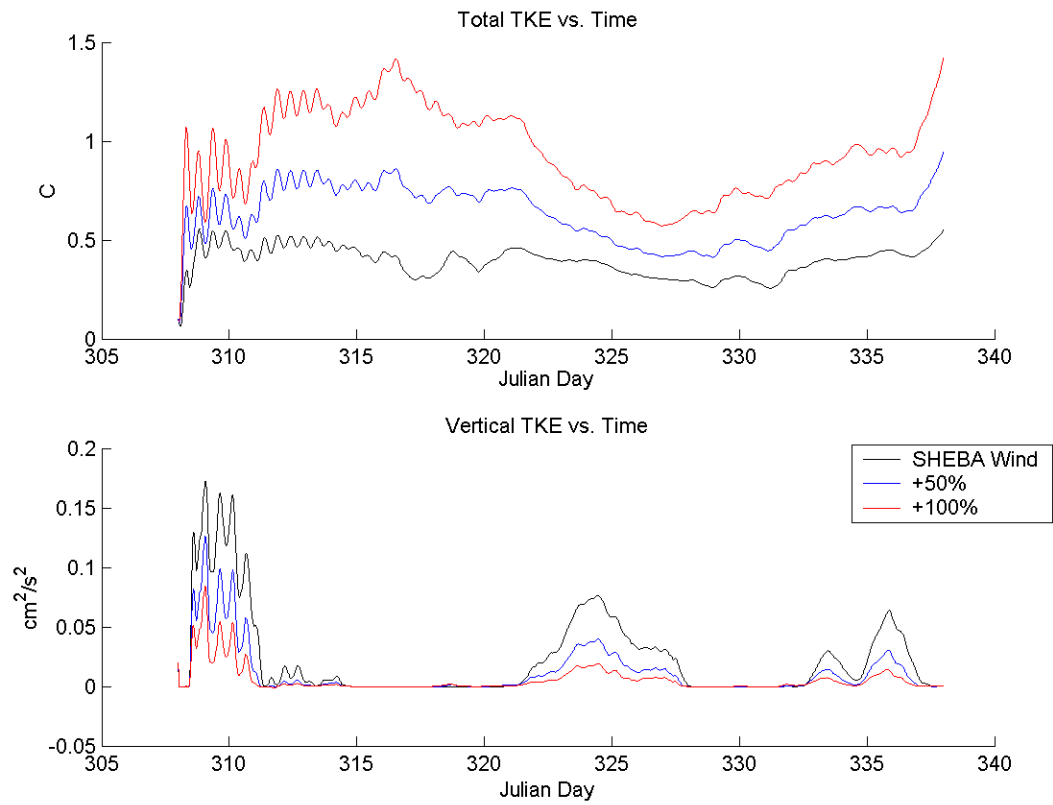


Figure 29. Total TKE and vertical TKE for vary wind speed.

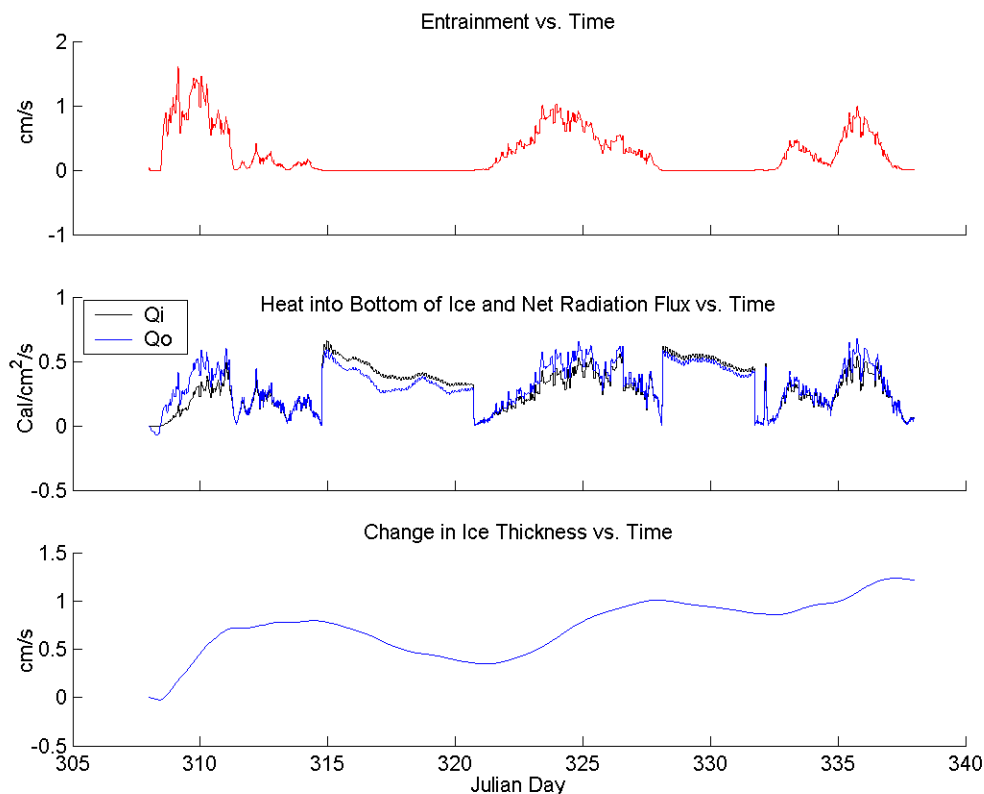


Figure 30. Sensitivity of net heat flux out and heat provided to the ice from the ocean

C. VARYING NET HEAT FLUX WITH THE SAME WIND SPEED

1. Simulation for Fifty Days

The effect of subtle changes in the net heat flux was studied by running the MICE model for fifty-days with net heat fluxes that varied $\pm 0.0002 \text{ Cal cm}^{-2} \text{ s}^{-1}$ from the original forcing with the same wind forcing and the same Greenland Sea temperature and salinity profiles. The SHEBA representative net heat flux (Figure 14) was used as a baseline control, case 1. For case 2, the net heat flux was decreased to represent a smaller amount of surface cooling due the presence of warmer air aloft. Finally, in case 3, the net heat flux was increased to represent additional surface cooling owed to evaporative cooling due to the presence of nearby open water or leads (Figure 31).

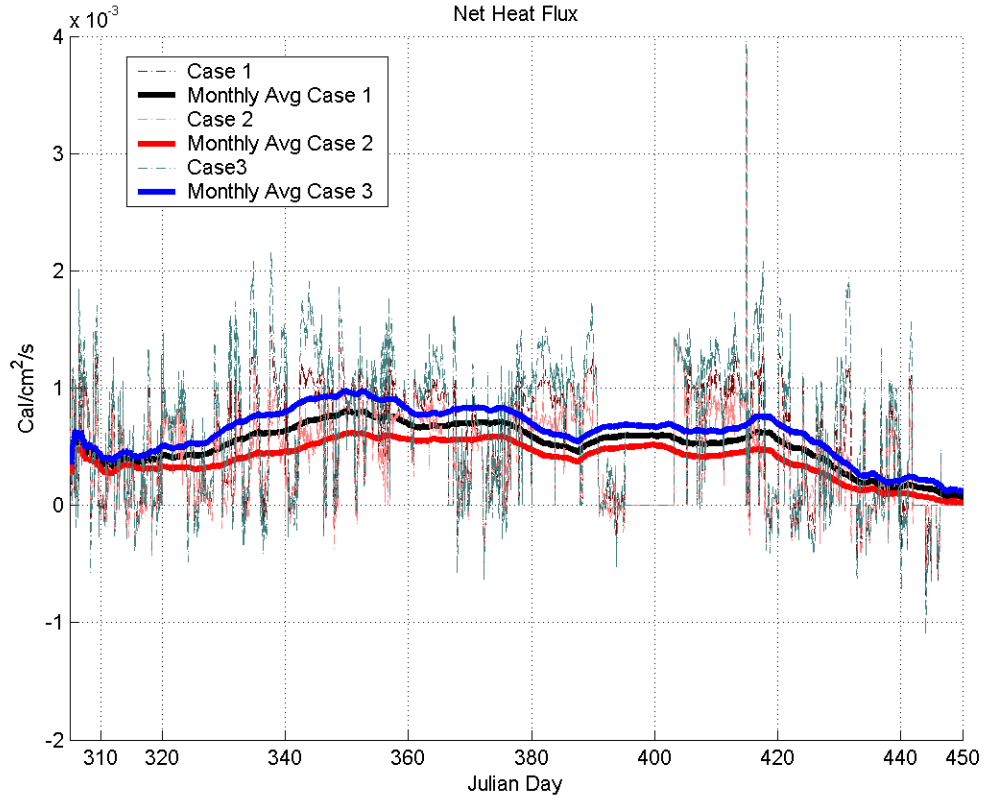


Figure 31. Three time series of net heat flux forcing during simulation.

As expected the results show the greatest entrainment in case 3 where the net upward surface heat flux was the largest, i.e. most cooling. The increased cooling in case 3 increased TKE and convection, which deepened the mixed layer 23.34 m over the fifty-day simulation. The mixed layer was 4.09 m deeper than case 1 and 8.69 m deeper than case 2 (Figure 32). Case 3 also formed the most ice, 3.98 cm, compared to the 3.15 cm and 2.21 cm of ice formed for case 1 and case 2 respectively. As a direct feedback to the ice freezing, salinity increased the most in case 3 due to increased brine rejection. Total TKE and vertical TKE for all cases appeared to fluctuate similarly, due to the identical wind forcing, but the numerical values of TKE have differences. The maximum cooling case had slightly greater total TKE and vertical TKE, whereas the least cooling case, case 2, had the least total and vertical TKE. Figure 33 shows case 3 had $0.013 \text{ cm}^2 \text{ s}^{-2}$ greater total TKE than case 1 and $0.027 \text{ cm}^2 \text{ s}^{-2}$ greater total TKE than case 2, and $0.016 \text{ cm}^2 \text{ s}^{-2}$ greater vertical TKE than case 1 and $0.033 \text{ cm}^2 \text{ s}^{-2}$ greater vertical TKE than case 2,

attributable to the increase in buoyancy flux by ice freezing. The differences between cases for heat storage in the mixed layer was a not result of the temperature flux into the bottom of the ice but due to the differences in temperature flux at the base of the mixed layer. As discussed earlier the temperature flux into the bottom of the ice varies with the square root of total TKE present in the system, \sqrt{E} . In this case the total TKE between cases was similar and therefore the temperature flux into the bottom of the ice was similar. As a result, in case 3 greater heat was stored in the mixed layer given that there was greater entrainment heat flux at the base of the mixed layer.

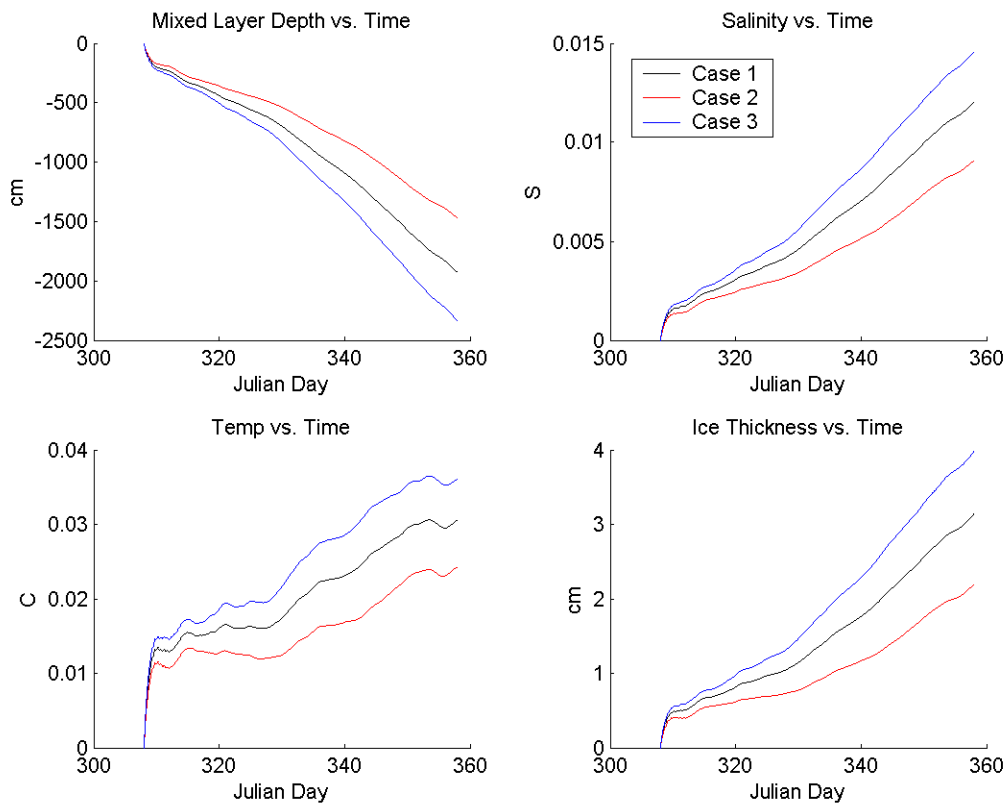


Figure 32. Varying net heat flux for the same wind speed.

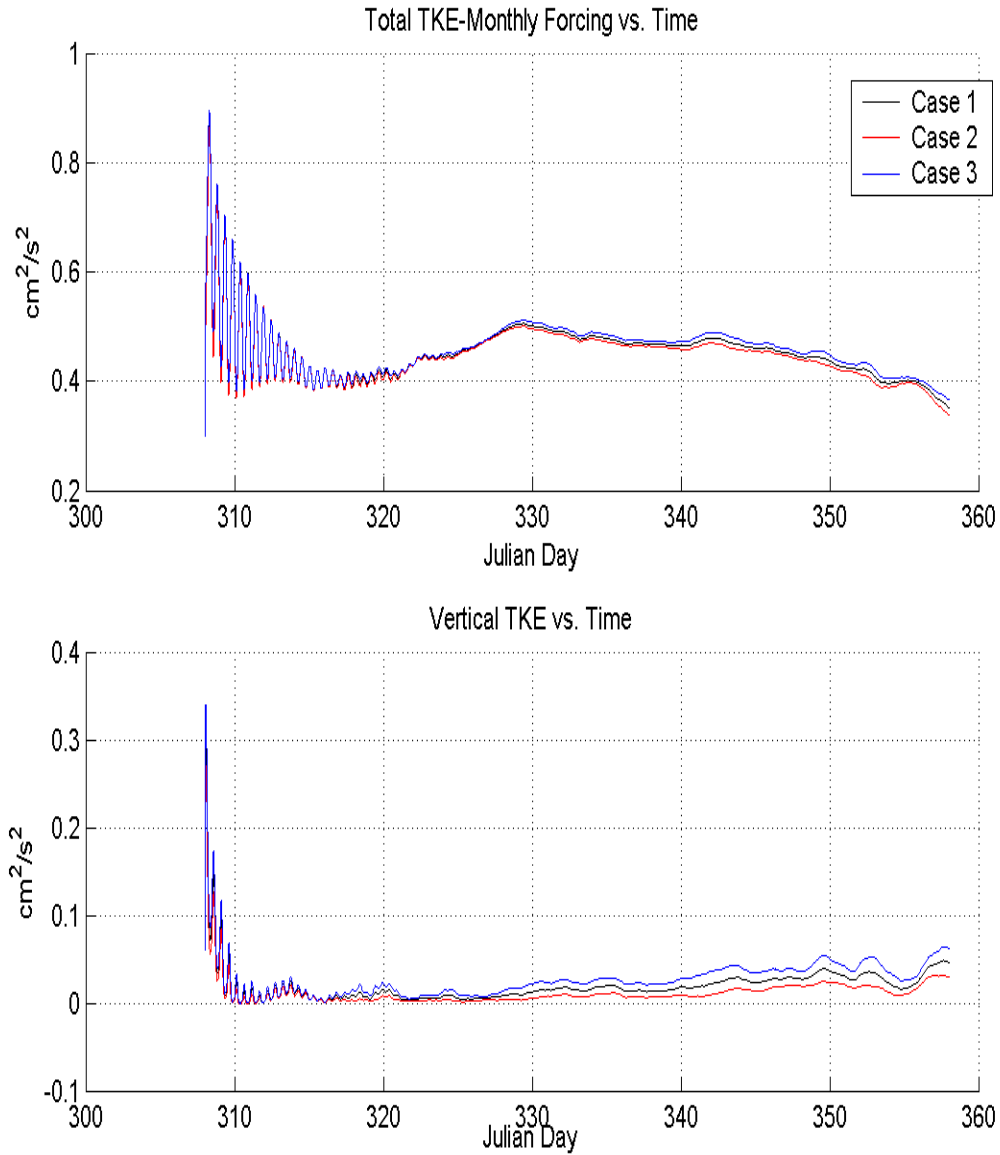


Figure 33. Total TKE and vertical TKE for vary net heat flux.

2. Simulation for One-Hundred and Fifty Days

Running cases 1, 2 and 3 for a longer period provides an indication of the sea-ice-air interactions which may be responsible for ice melting and the formation of polynyas and leads despite a positive heat flux averaged throughout the period.

Figure 31 shows the monthly averaged net heat flux forcing during the one-hundred and fifty-day period. Throughout the model run, the net heat flux was always positive and the system remained in a deepening regime. Ice begins to melt in all cases at Julian Day 424. After Julian Day 424 the entrainment in all cases was strongly damped due to the negative buoyancy flux in the mixed layer from the stratifying effect of the fresh water input due to ice melting (Figure 34-35). As shown in the mixed layer temperature plot (Figure 34), the mixed layer continues to provide heat to the underside of the ice during the damped entrainment periods by reducing the heat storage in the mixed layer and fluxing it into the ice bottom. The feedback due to ice melting is illustrated in Figure 36 and Figure 37. Figure 36 shows the ice transitioning on short time scales between freezing and melting in response to the atmosphere forcing and ocean feedback. Figure 37 illustrates the natural damping effect on vertical TKE, and thereby entrainment, due to the ice melting.

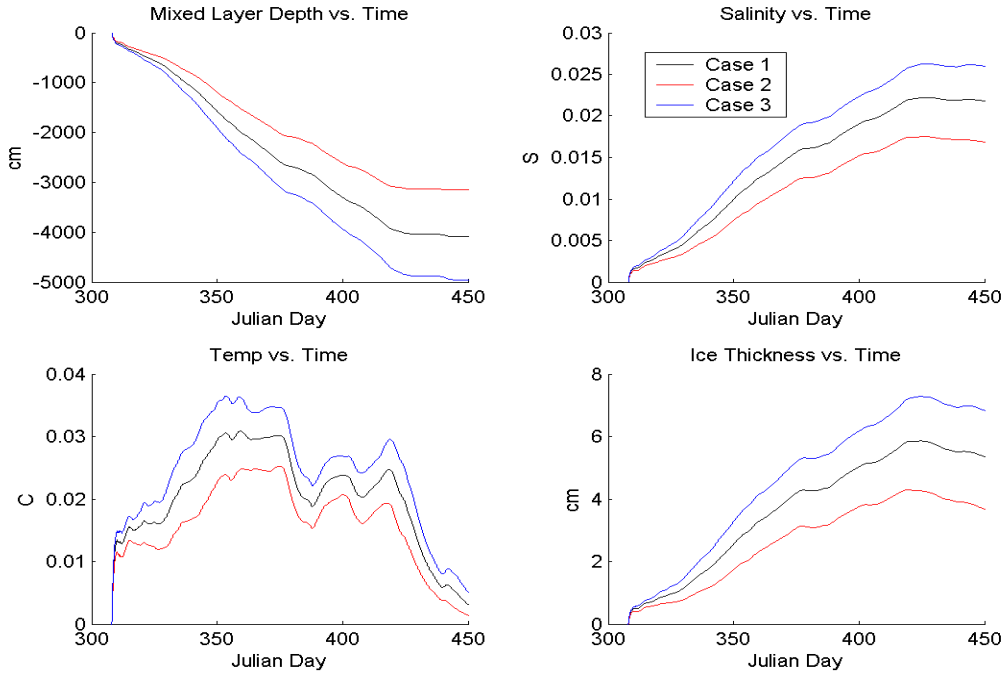


Figure 34. Ice melting despite atmospheric cooling

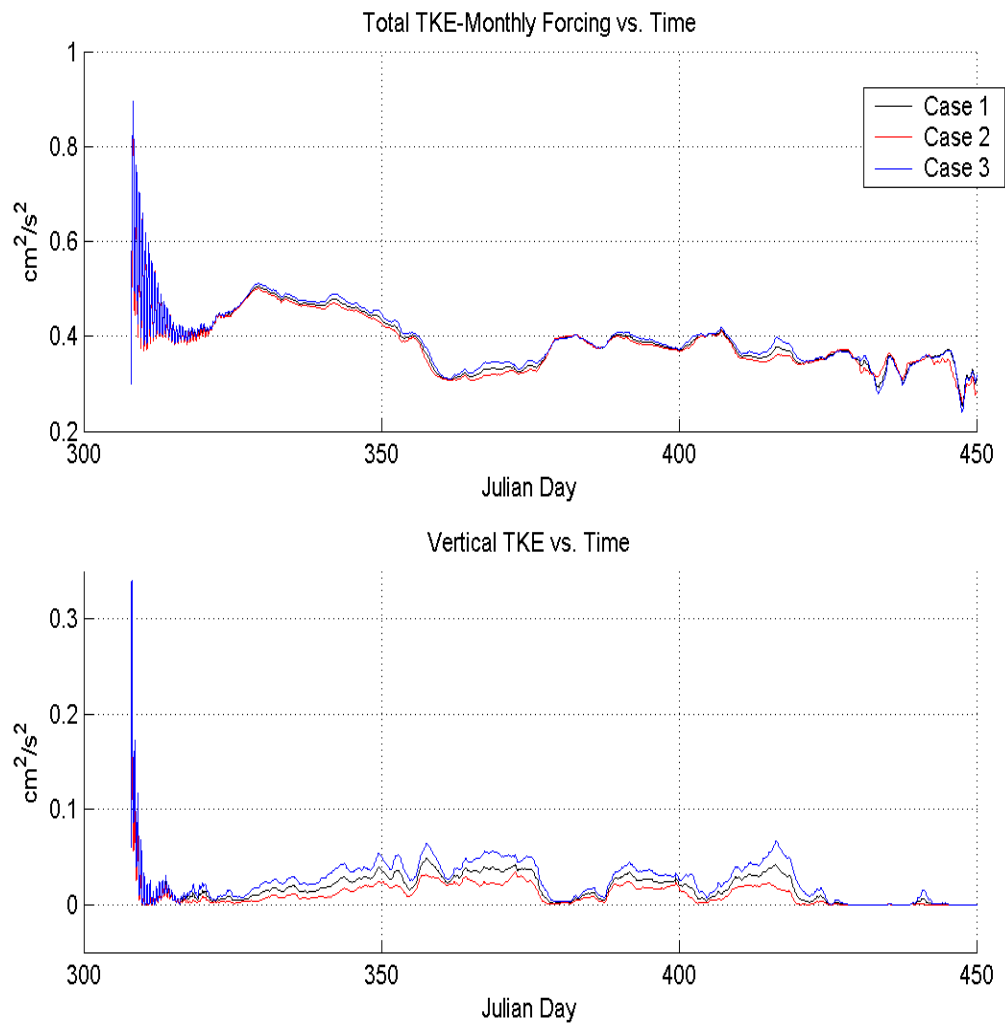


Figure 35. Entrainment is damped in response to the negative buoyancy flux in the mixed layer resulting from ice melting.

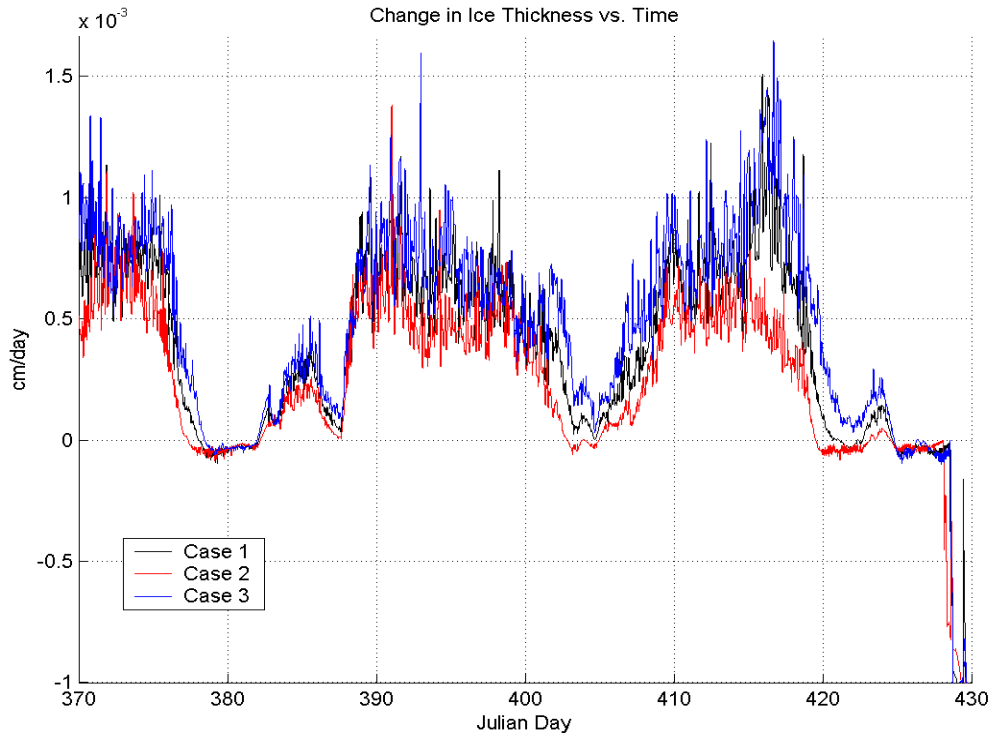


Figure 36. Ice transitioning on short time scales between freezing and melting periods in response to the atmosphere forcing and ocean feedback.

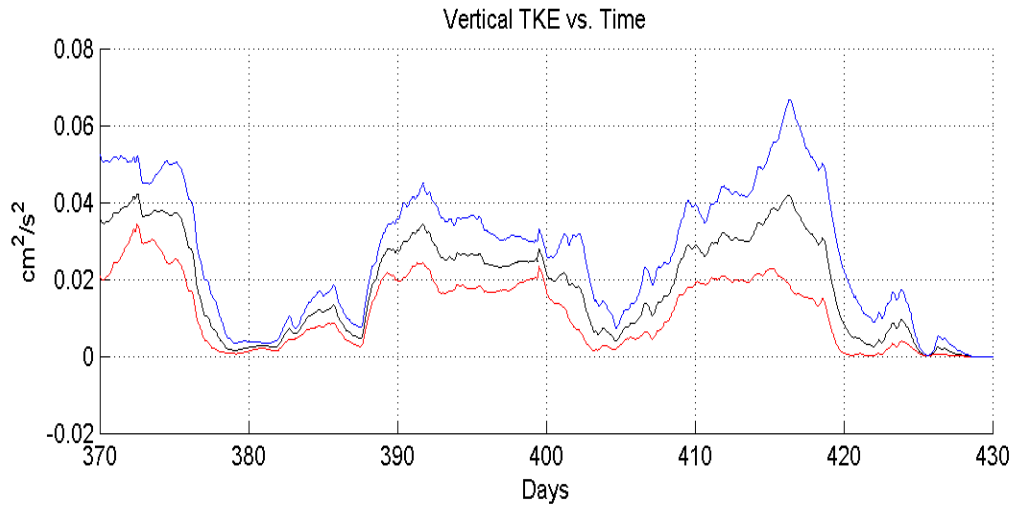


Figure 37. Damping effect on vertical TKE due to the ice melting.

D. ATMOSPHERIC FORCING

To address the relative effect that temporal resolution of the forcing data has on the model skill, a moving average was applied to the SHEBA atmospheric data to produce four time-series, representative of hourly, daily, weekly and monthly forcing (Figure 34-35). The Western Arctic and Greenland Sea temperature and salinity profiles were simulated for fifty days forced with each of the four time-series of atmospheric data.

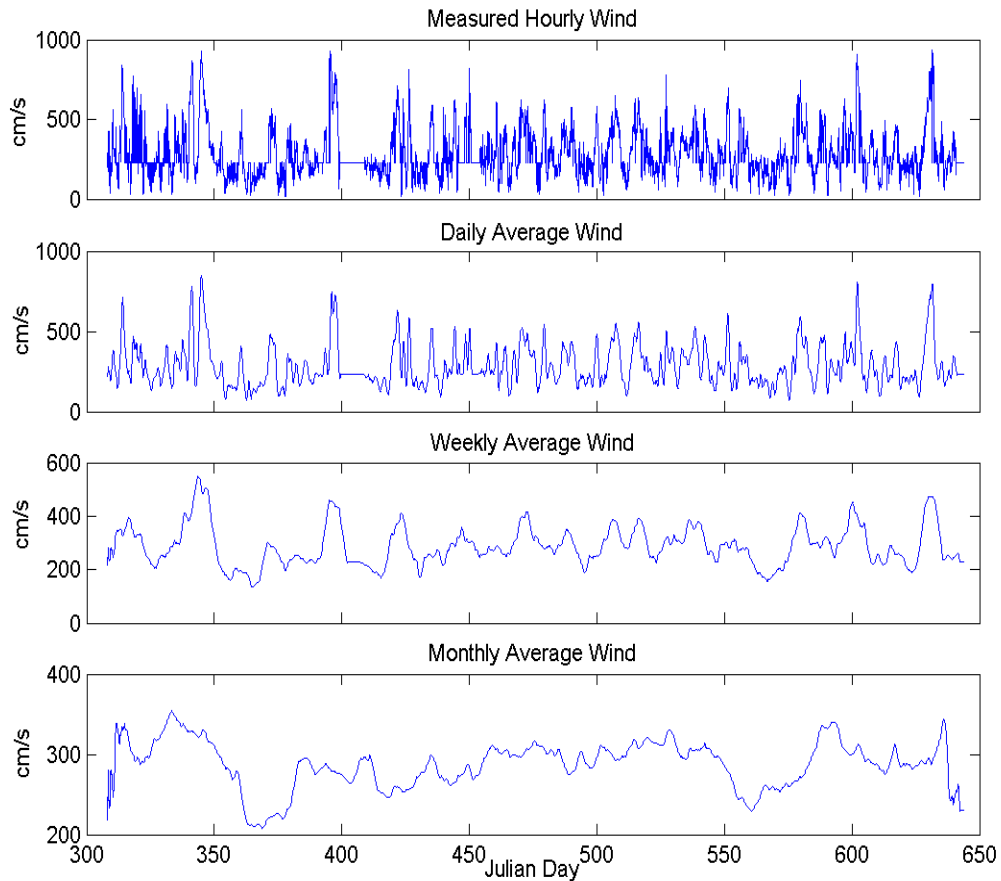


Figure 38. Moving average applied to wind forcing

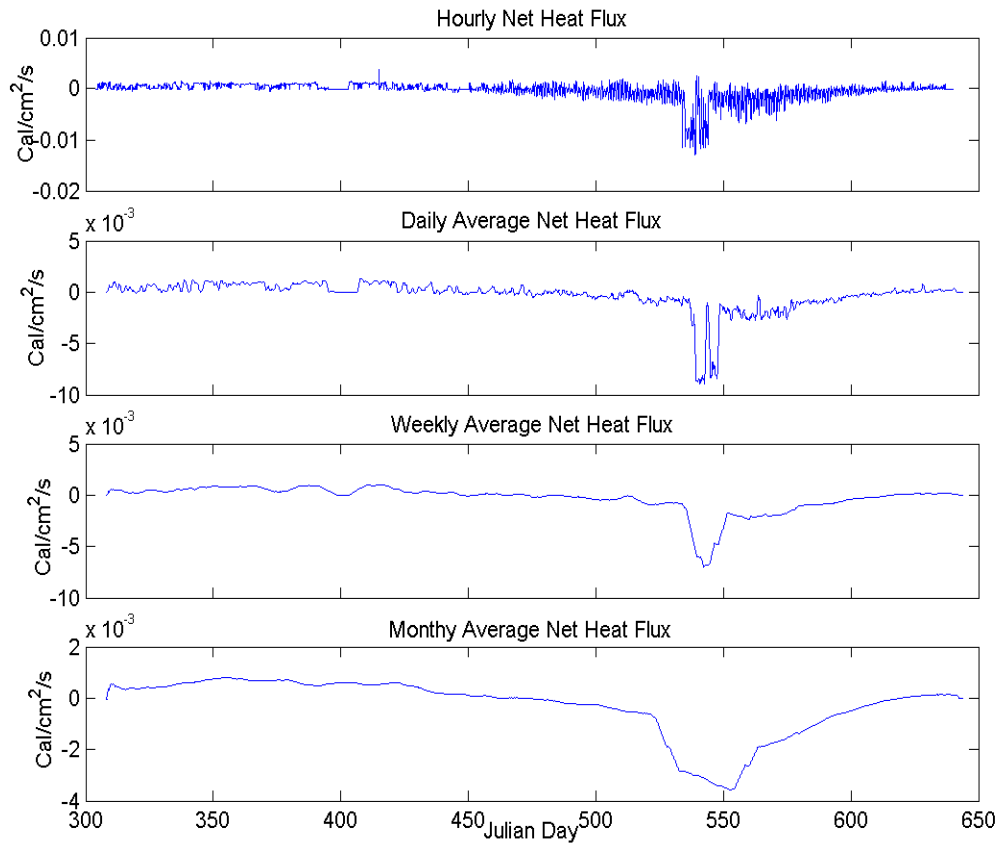


Figure 39. Moving average applied to net heat flux

The plots from both cases show the results over the fifty-day period to be in general agreement (Figure 36-37). However, there are differences on a time scale shorter than one to two days. The differences can be attributed to the fluctuation in TKE between the different forcing time-series data. Examining the plots of total turbulent kinetic energy for the Western Arctic and Greenland Sea model runs reveals that there are negative energy values predicted in both the hourly forced and daily forced cases (Figure 38-39). Negative energy is unphysical. Here TKE is being converted to potential energy (PE), and the turbulence in the mixed layer cannot reach the base of the earlier established mixed layer. This is a period where the system is attempting to switch from a deepening regime to a shoaling regime. The Greenland Sea, having a deeper mixed

layer, has larger negative values of TKE because the amount of shoaling, or retreating, is greater.

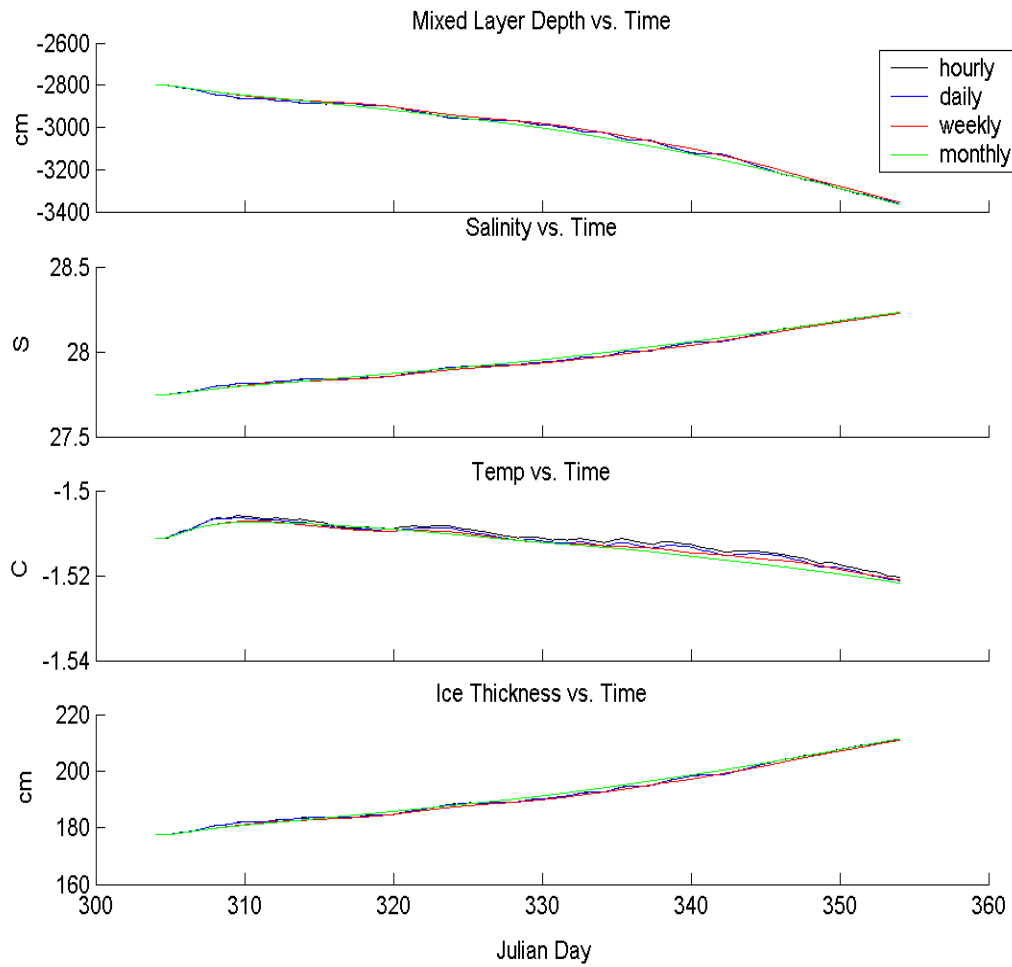


Figure 40. Western Arctic MICE simulation

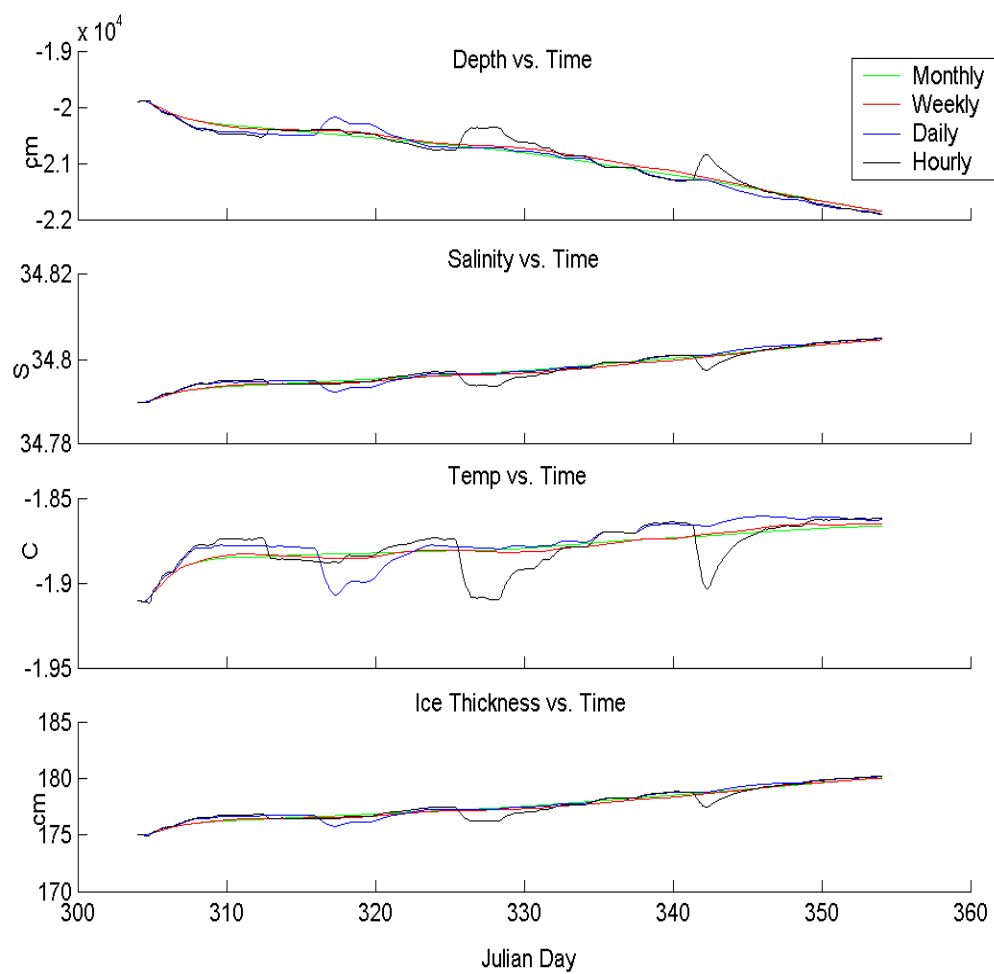


Figure 41. Greenland Sea MICE simulation

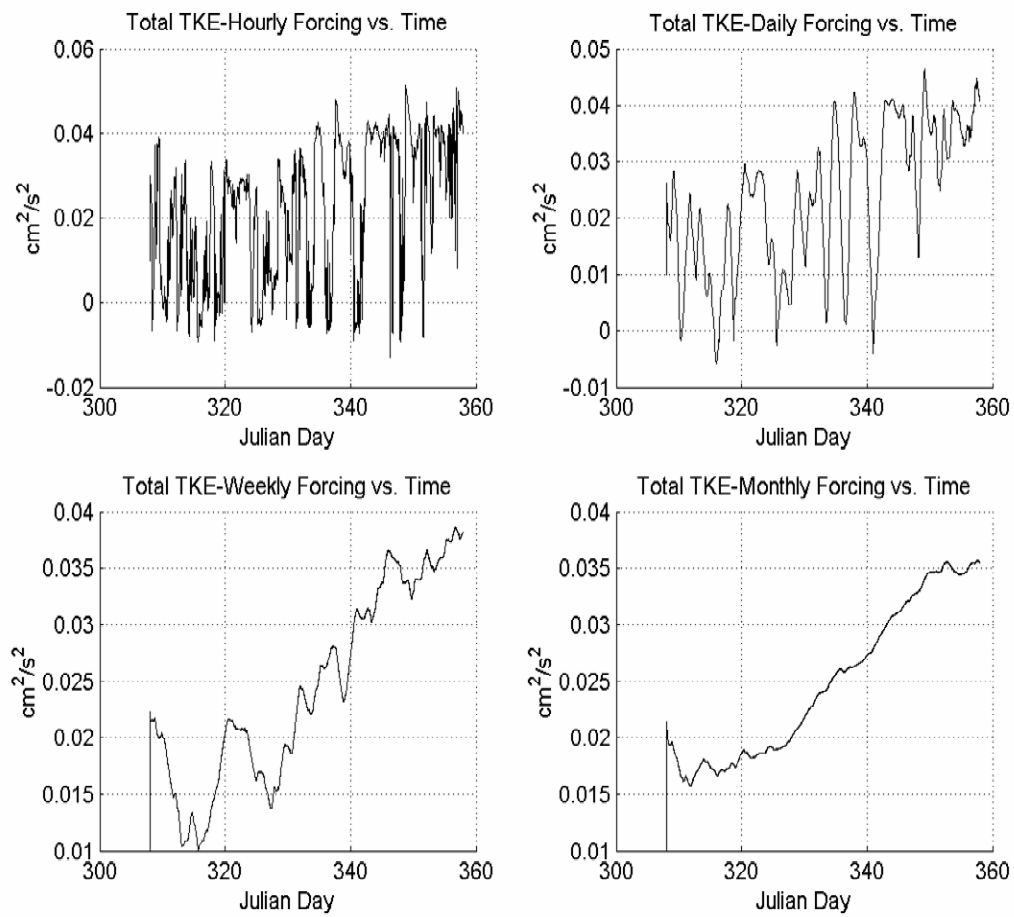


Figure 42. Western Arctic Total TKE

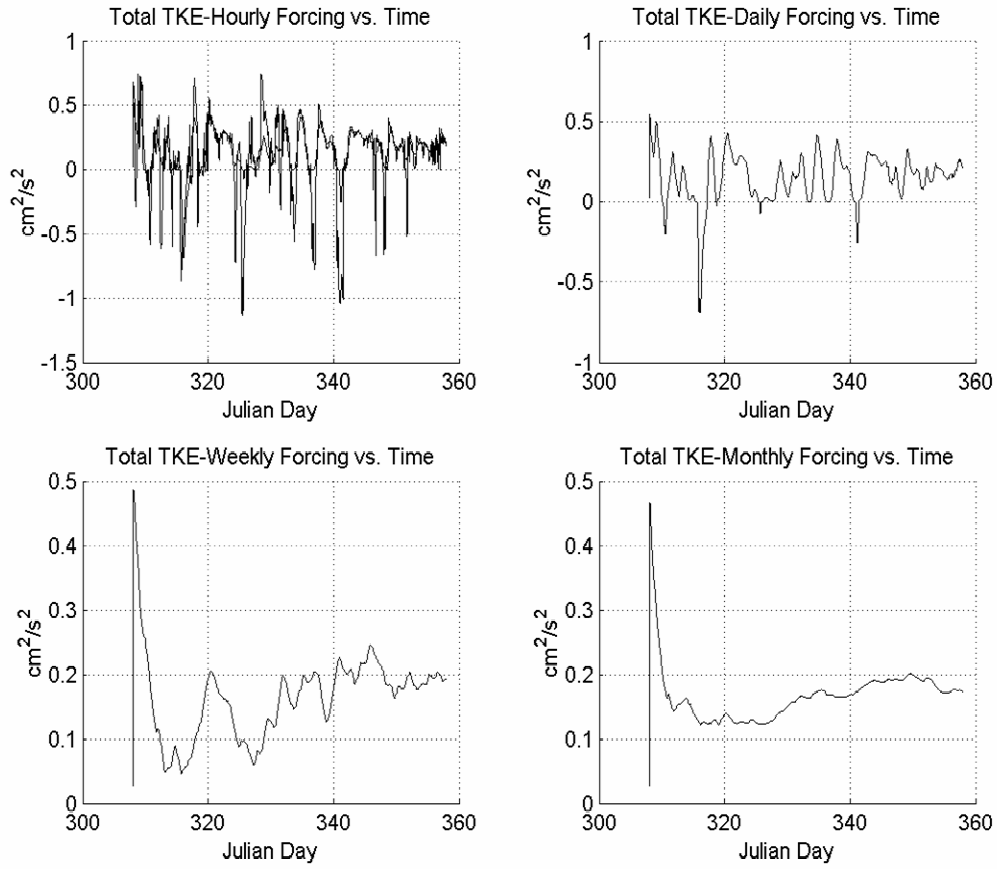


Figure 43. Greenland Sea Total TKE

1. Retreating Regime

The model can be used as a diagnostic tool to predict the changing regimes. Understanding that water cannot be unmixed or “unentrained”, a retreating MICE model was developed to solve the system of equations under a shoaling regime. In the retreating version of the MICE model, entrainment is set to zero, and the mixed layer depth is diagnostically prescribed equal to the Obukhov length scale, $h = L = \frac{u_*^3}{b'w'_0}$. The effect

of this is a mixed layer decoupled from the underlying ocean. The ice will still receive heat from the mixed layer if there was previous heat storage in the mixed layer, but under the shoaling regime the atmospheric forcing plays a dominant role.

The Greenland Sea daily atmospheric forcing case was run for a seventeen-day period using the retreating version of the MICE model during the periods where negative

TKE was predicted. Figure 40 shows the negative energy values occurring during three periods, Julian day: 310, 315, and 319. The models were run to time indicated by the dash blue line. Examining Figure 41 reveals similar system tendencies on the longer time scale but on the shorter period the importance of changing regimes are clear and significant.

A good example of the decoupling of the heat source of the deep ocean is at Julian day 315. Without the entrainment zero, the system tries to “unentrain” temperature and salinity, which is not physically realistic. Furthermore, the model predicts ice melting. Applying the same forcing to a proper retreating model, no ice is melted and the mixed layer temperature and salinity budgets are corrected.

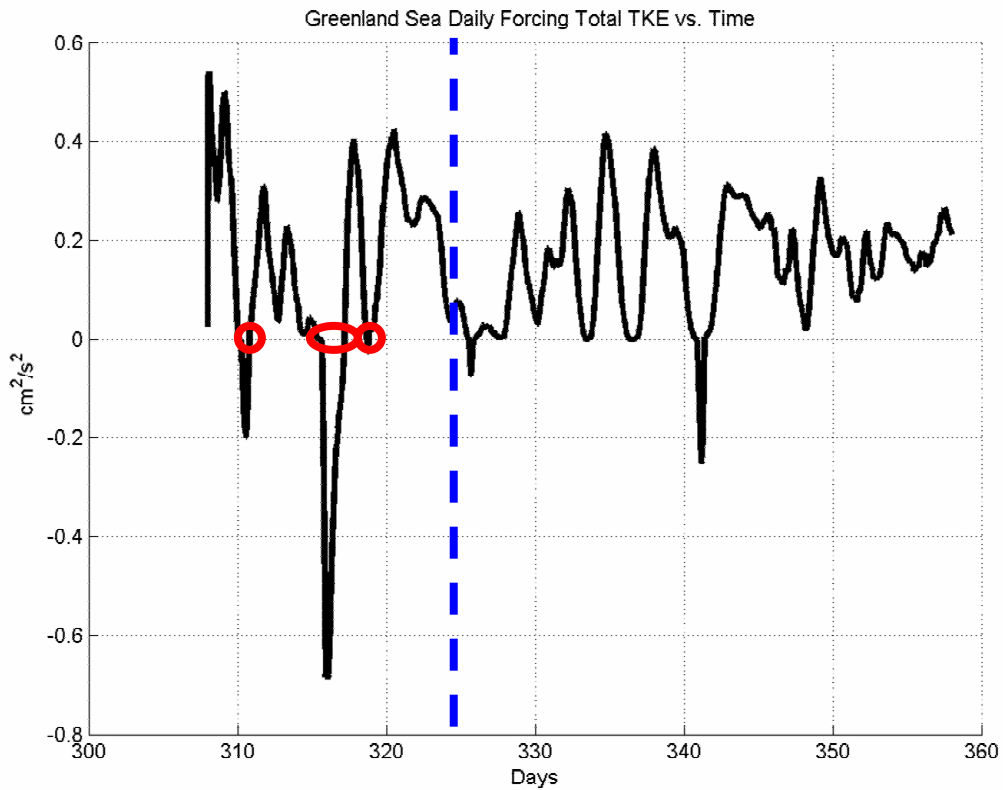


Figure 44. Greenland Sea Daily Forcing Total TKE

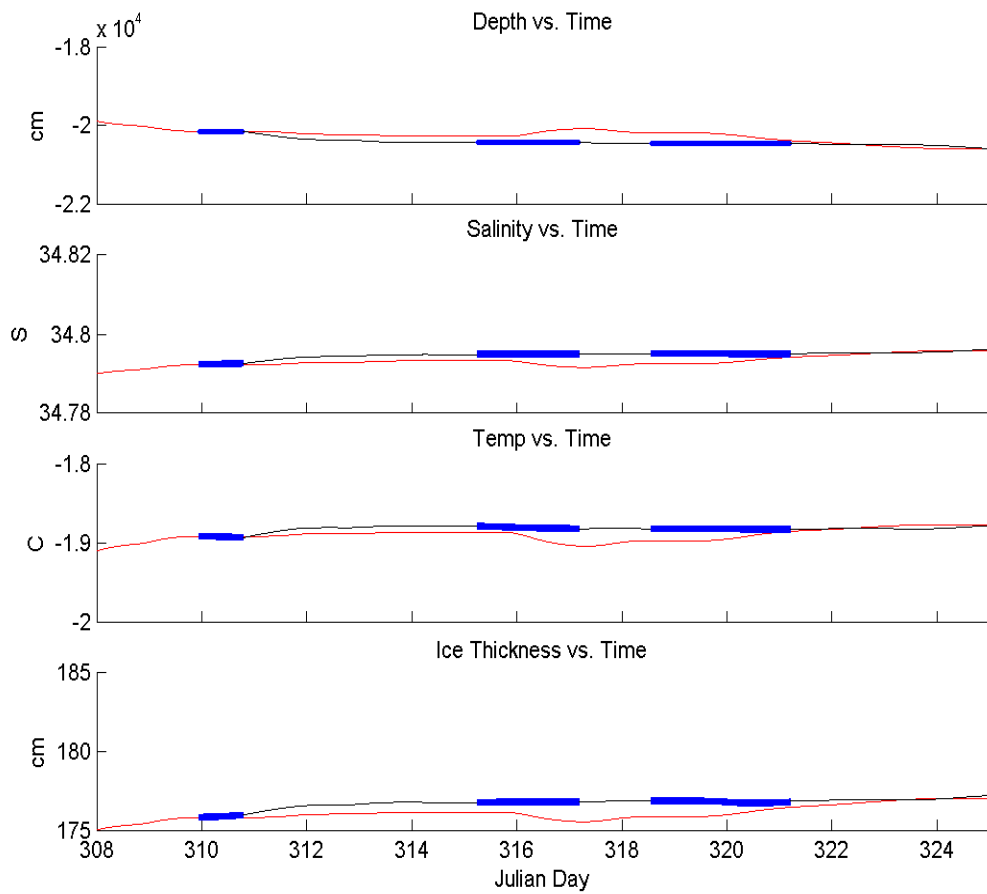


Figure 45. Greenland Sea Daily Forcing MICE Model vs. Model verses Retreating Version

THIS PAGE INTENTIONALLY LEFT BLANK

V. CONCLUSIONS

A. SUMMARY

A turbulent kinetic energy (TKE) budget model of a coupled sea-ice-air mixed layer system including realistic thermodynamics is vital to the accurate prediction of ice-open water boundaries, polynyas, and coastal and deep-water formation in the polar sea. This work illustrates the complexity of sea-ice-air interactions, and the short time scale upon which the mixed layer responds to changes in forcing conditions. There is no single factor that is most important in predicting high latitude sea-ice-air interactions because the dynamics within the mixed layer are a result of the sea-ice-air system interaction as a whole. The state of the ice cover changes in response to forcing from a closely coupled atmosphere and ocean.

While the atmosphere generally governs the regime type, deepening or shoaling, the ocean's role cannot be considered separately. In the deepening regime the ocean plays a large role due to entrainment but also plays a role during shoaling periods due to the heat storage capacity of the mixed layer. The MICE model allows a deeper understanding of the limits and the relative importance of the different contributors to the heat, momentum, salinity, and TKE budgets. Prediction of buoyancy flux, shear production, dissipation, and entrainment as functions of local surface forcing shed light on the intrinsic feedbacks within the coupled system.

It was shown that changes in initial conditions such as mixed layer depth, and temperature and salinity profiles of the polar oceans have significant effects on the prediction of ice formation or melting. Increases or decreases in the atmospheric forcing may have unintuitive effects that only a realistic coupled system can predict. When modeling ice thickness and the temperature and salinity profiles on short time scales, as used operationally in tactically relevant problems such as undersea warfare or surface warfare, the atmospheric forcing time scale is crucial to accurate prediction of short-term regime changes that would be missed by coarser resolution forcing.

This work demonstrates that ice extent forecast models such as the U.S. Navy PIPS model potentially could be significantly improved by incorporating small time scale

atmospheric forcing and underlying ocean structure in concert with parameterization from the more complete physics contained in the MICE model.

B. RECOMMENDATIONS FOR FURTHER STUDY

Currently the Matlab® version of the MICE model cannot automatically transition between deepening and shoaling regimes without user intervention. Enhancing the Matlab® MICE model to diagnose regime changes and adjust mixed layer depth, temperature profile and salinity profile would increase the model capabilities and ease of use.

Further insight into the nonlinear physics and the complex relationships of the mixed layer dynamics can be gained by running the MICE model against other atmospheric forcing and ocean profile observations from the Arctic and its marginal seas.

The results of this testing and analysis can provide further guidance and verification for the development of the parameterization of heat flux, momentum flux, salinity flux, and TKE budgets from a one dimensional model to three dimensional ocean models to predict basin and larger-scale sea-ice-air interactions.

LIST OF REFERENCES

Aagaard, K. and E.C. Carmack. The arctic ocean and climate: a perspective, in *The Role of the Polar Oceans in Shaping the Global Environment*, O. Johannessen, R. Muench and J. Overland, Eds., Geophysical Monograph 85, pp.5-20, 1994.

AMAP Assessment Report: Arctic Pollution Issues- Chapter 2: Physical/Geographical Characteristics of the Arctic, 1998.

Barry, R.G., M.C. Serreze, J.A. Maslanik, and R.H. Preller. The arctic sea ice-climate system: observations and modeling. *Review of Geophysics*, 31, 397-422, 1993.

Barry, R.G. and F.K. Hare, Arctic and Alpine environments, pp. 17-54. Methuen, London, 1974.

Bramson, L. S., *Air-Sea Interactions and Deep Convection in the Labrador Sea*, Master's Thesis, Naval Postgraduate School Monterey, California, December 1997.

Chu, P.C. and R.W. Garwood, Jr. Comment on 'A coupled dynamic-thermodynamic model of an ice-ocean system in the marginal ice zone' by S. Hakkinen. *J. Geophys. Res.*, 93, 5155-5156, 1988.

Coachman, L.K. and K. Aagaard, Physical Oceanography of Arctic and Subarctic Seas, Chapter 1, in *Marine Geology and Oceanography of the Arctic Seas*, Y. Herman, ed., 1-72, Springer-Verlag, N.Y., 1974.

Garwood, R.W., Jr. An oceanic mixed layer model capable of simulating cyclic states. *J. Phys. Oceanogr.*, 7, 455-471, 1977.

Garwood, R.W., Jr. Enhancements to deep turbulent entrainment. In *Deep Convection and Deep Water Formation in the Ocean*, Ed. by P. C. Chu and J. C. Gascard, Elsevier, 189-205, 1991.

Garwood, R.W., Jr. Missing physics for deep convection? Arctic System Science Ocean-Atmosphere-Ice Interactions Modeling Workshop, Pacific Grove, Report No. 1, 49-54, 1992.

Garwood, R.W., Jr. Oceanic convective instabilities hypothesized, *ARCSS-OAII Newsletter*, 2, 4-5, 1992.

Garwood, R.W., Jr. Critical mixed layer depth for maintaining convective polynyas. International Polynya Symposium, Quebec City, September, 2001.

Garwood, R.W., Jr. Thermodynamics Critical to Arctic Mixed Layer Systems, Small-Scale Sea Ice Ocean Modeling (SIOM) Workshop, Fairbanks, August, 2002.

Garwood, R.W. "MICE (Mixed layer-ICE) Coupled Model' Unpublished Report, March 2004.

Garwood, R.W., Jr., S.M. Isakari, and P.C. Gallacher. Thermobaric convection, in *The Role of the Polar Oceans in Shaping the Global Environment*, O. Johannessen, R. Muench and J. Overland, Eds., Geophysical Monograph 85, pp.199-209, 1994.

Harder, M., and P. Lemke, Modelling the extent of sea ice ridging in the Weddell Sea, *The Polar Oceans and Their Role in Shaping the Global Environment*, Geophysical Monograph, 85, AGU, Washington, USA, 187-197, 1994.

Hakkinen, S. A coupled dynamic-thermodynamic model of an ice-ocean system in the marginal ice zone. *J. Geophys. Res.*, 92, 9469-9478, 1987.

Hibler, W.D.. A dynamic thermodynamic sea ice model. *J. Phys. Oceanogr.*, 9, 817-846, 1979.

Kraus, E.B. and J.A. Businger. Atmosphere-Ocean Interaction (2nd Ed.). *Oxford Univ. Press*, 1994.

Kraus, E.B. and J.S. Turner. A dynamic thermodynamic sea ice model. *Tellus*, 19, 98-105, 1967.

Lemke, P., W.B. Owens and W.D. Hibler, III. A coupled sea ice-mixed layer - pycnocline model for the Weddell Sea. *J. Geophys. Res.*, 95, 9513-9525, 1990.

Lipscomb, W.H. Modeling the Thickness Distribution of Arctic Sea Ice. PhD thesis, Dept. of Atmospheric Sciences, Univ. of Washington, Seattle, 1998.

Lumley, J. L., and B. Khajeh-Nouri, Computational modeling of turbulent transport. *Advances in Geophysics*, Vol 18A, Academic Press, 169-192, 1974.

Macdonald, R.W. and J.M. Bowers, Contaminants in the Arctic marine environment: priorities for protection. *ICES J. Mar. Sci.* 53: 537-563, 1996.

Mellor, G L. And T. Yamada, Development of a turbulence closure model for geophysical fluid problems. *Rev. Geophys.*, 20, 8510875, 1982.

Niiler, P.P. Deepening of the wind mixed layer. *J. Mar. Res.*, 33, 405-422, 1975.

NOAA, Data Announcement 88-MGG-02, Digital relief of the surface of the Earth. NOAA, National Geophysical Data Center, Boulder, Colorado, 1988.

Persson, O. P. G. Persson, C. W. Fairall, E. L. Andreas, P. S. Guest. Measurements near the Atmospheric Surface Flux Group tower at SHEBA: Near-surface conditions and surface energy budget, *J. Geophys. Res.*, 107, C10, SHE 13, 2002.

Quadfasel, D. and M. Ungewß, MIZEX 87 - RV Valdivia Cruise 54, CTD Observations in the Greenland Sea, *Technical Report 5-88*, Institut für Meereskunde der Universität Hamburg, 1988.

Roth, M. K., *Effects of Thermobaricity on Coupled Ice-Mixed Layer Thermodynamics*, Master's Thesis, Naval Postgraduate School Monterey, California, June 2003.

Smith, S.D., R.D. Muench, and C.H. Pease. Polynyas and leads: An overview of physical processes and environment. *J. Geophys. Res.*, 95, 9461-9479, 1990.

SHEBA Phase 2 Data Sets, "SHEBA: Ice Camp CTD Time Series (Matlab®) (Stanton), Model Ice Deformation and Ice Thickness Distribution, Tower, 5-level hourly measurements plus radiometer and surface data at Met City (ASFG)." [<http://www.joss.ucar.edu/sheba/webresponse/sheba2.html>]. Sept 04.

SHEBA Principal Investigators, "Phase 2 and Phase 3 Investigators." [<http://sheba.apl.washington.edu/sheba3/directories/Ph2andPh3PIs.html>]. Sept 04.

SHEBA Map of Ice Station Drift, "Ice Station." [http://sheba.apl.washington.edu/sheba3/icestation/ice_tracks.gif]. Sept 04.

USSR Ministry of Defense, The Atlas of the Oceans - Arctic Ocean. USSR Ministry of Defense, 1980.

Weingartner, T., University of Alaska Institute of Marine Science, "Chukchi Sea Circulation." [<http://www.ims.uaf.edu/chukchi/>]. Sept 04.

Woodgate, R.A., K. Aagaard, and T. Weingartner, A Year in the Physical Oceanography of the Chukchi Sea: Moored measurements from Autumn 1990-1991. *Deep-Sea Research*, 2004.

THIS PAGE INTENTIONALLY LEFT BLANK

INITIAL DISTRIBUTION LIST

1. Defense Technical Information Center
Ft. Belvoir, Virginia
2. Dudley Knox Library
Naval Postgraduate School
Monterey, California
3. Chairman
Department of Oceanography
Naval Postgraduate School
Monterey, California
4. Chairman
Department of Meteorology
Naval Postgraduate School
Monterey, California
5. Office of Naval Research
Code 322PO
Atten: Dr. Theresa Paluszkiewicz
800 North Quinct Street
Arlington, Virginia 22217-5660
6. Prof. Roland W. Garwood
Department of Oceanography
Naval Postgraduate School
Monterey, California
7. Arlene Guest
Department of Oceanography
Naval Postgraduate School
Monterey, California
8. LT William A. Swick
NAVPACMETOCCEN
San Diego, California